The Journal of Chemical Physics

RESEARCH ARTICLE | JULY 23 2026

Cooperative stability, many-body expansion, and σ-aromaticity of $(LiH)_n$ clusters (n = 1–6): A CCSD(T) study at the complete basis set limit

Emmanouil Semidalas ; Filippos Drakopoulos ; E. Alexandros Routsi ; Demeter Tzeli

J. Chem. Phys. 165, 044306 (2026)
https://doi.org/10.1063/5.0336948

The Journal of Chemical Physics ARTICLE pubs.aip.org/aip/jcp

Cooperative stability, many-body expansion, and σ-aromaticity of $(LiH)_n$ clusters (n = 1–6): A CCSD(T) study at the complete basis set limit

Cite as: J. Chem. Phys. 165, 044306 (2026); doi: 10.1063/5.0336948
Submitted: 3 April 2026 • Accepted: 2 July 2026 •
Published Online: 23 July 2026

Emmanouil Semidalas,[1,a] Filippos Drakopoulos,[1] E. Alexandros Routsi,[1,2] and Demeter Tzeli[1,3,a]

AFFILIATIONS

[1] Laboratory of Physical Chemistry, Department of Chemistry, National and Kapodistrian University of Athens, Panepistimiopolis Zografou, Athens 15784, Greece
[2] Laboratory of Organic Chemistry, Department of Chemistry, National and Kapodistrian University of Athens, Panepistimiopolis Zografou, Athens 15784, Greece
[3] Theoretical and Physical Chemistry Institute, National Hellenic Research Foundation, 48 Vassileos Constantinou Ave., Athens 11635, Greece

[a] **Authors to whom correspondence should be addressed:** emmanous@chem.uoa.gr and tzeli@chem.uoa.gr

ABSTRACT

We investigated the energetics and bonding of lithium hydride clusters $(LiH)_n$ (n = 1–6) using a composite *ab initio* scheme inspired by W2 theory to achieve sub-kcal/mol accuracy. This approach combines CCSD(T) results extrapolated to the complete basis set limit with a rigorous treatment of core–valence correlation, scalar relativistic effects, and the diagonal Born–Oppenheimer correction. Our results show that while Hartree–Fock theory captures the primary electrostatic binding, correlation effects are crucial for determining the energetic preference of compact isomers over cyclic rings. A parallel density functional theory study shows that while standard hybrid functionals like B3LYP-D4 and M06-2X exhibit larger deviations, the double-hybrid revDSD-PBEP86-D4 functional closely matches our benchmarks, delivering sub-kcal/mol accuracy. Structural and chemical bonding analyses, including intrinsic bond orbital, nucleus-independent chemical shift, and many-body expansion (MBE) methods, reveal high ionic character and multi-center bonding (3c–2e and 4c–2e) within the $(LiH)_n$ clusters. MBE analysis of the interaction energy of the monocyclic clusters with respect to the LiH molecules reveals that the two- and three-body terms are consistently negative (stabilizing), while all higher-order terms are negligible. We find that σ-aromaticity in these systems is predominantly local and bond-centered. As the rings expand, the interior becomes magnetically decoupled from the σ-skeleton, precluding the formation of a global ring current. These results establish definitive benchmarks for the stability of prototypical electron-deficient clusters.

I. INTRODUCTION

Lithium hydride (LiH) and its clusters serve as prototypical systems for investigating ionic bonding and electron-deficient frameworks. As the simplest heteronuclear diatomic molecule, the LiH molecule has been well characterized spectroscopically and theoretically (see Ref. 1 and references therein) due to its important role in early-universe chemistry.[2–4] Theoretical studies have thoroughly examined the formation pathways, abundance, and possible role of LiH as a coolant in collapsing primordial gas clouds.[5–8] Furthermore, a significant body of theoretical work[9–18] has mapped the potential energy surfaces (PES) of small related species, such as protonated LiH_2^+, in its ground and excited electronic states, Li_2 (see Ref. 19 and references therein), Li_2^+, and Li_2^-.[20,21] In the condensed phase, LiH is a crystalline solid that serves as a reagent in organic synthesis, as a neutron moderator or shielding material in nuclear reactors,[22] and as a proposed candidate for hydrogen storage applications.[23–25] Electronic structure methods have also been extended to the solid state; for instance, Manby *et al.*[26] considered a molecular cluster-based scheme for accurate cohesive energies and enthalpies of formation for the LiH crystal at the second-order Møller–Plesset perturbation level of theory (MP2)

and the CCSD(T)[27,28] level (i.e., coupled cluster with all singles, doubles, and quasi-perturbative triple excitations). Bridging the gap between these isolated diatomic molecules and the bulk crystal, small lithium hydride $(LiH)_n$ clusters provide an ideal model for exploring structural and charge-transfer effects.

Experimentally, Broyer and co-workers[29,30] characterized $(LiH)_n$ clusters using photoionization, absorption cross-section measurements, and time-of-flight mass spectrometry (TOF-MS). These studies revealed that the bonding is ionic and that the evaporative rates provided strong evidence for metal–insulator segregation in metal-rich clusters, where a metallic Li_{n-m} core remains largely unperturbed by an insulating $(LiH)_m$ shell. These findings also confirmed that hydrogen atoms bind preferentially to the cluster surface rather than penetrating the interior. Notably, $(LiH)_n$ and $(LiH)_nLi_3^+$ clusters were the most abundant species. "Magic-number" stabilities of $Li_p(LiH)^+_q$ clusters coincide with those of purely metallic Li_p^+ clusters (p = 9 and 21), which can be explained by the jellium model. It was also reported that the $Li_nH_m^+$ clusters fragment by ejecting LiH or LiH_2.[29–31] Complementary insights for small $(LiH)_n$ clusters (n = 2,3,4) were reported by Wang and Andrews[32] via matrix-isolation infrared spectroscopy. They identified these small $(LiH)_n$ clusters following the reaction of laser-ablated lithium atoms with H_2 in *para*-hydrogen, neon, and argon matrices.

On the theoretical side, most studies on $(LiH)_n$ clusters have investigated their equilibrium geometries, energetics, and spectroscopic properties employing semiempirical methods, density functional theory (DFT), and low-level wavefunction methods. For example, an early study[33] reported the optimized structures of $(LiH)_n$ clusters ($n \leq 8$) at the Hartree–Fock level, their stabilization energies per LiH molecule, and their ionization potentials, showing that odd number n structures are planar [e.g., the cyclic trimer $(LiH)_3$] while larger structures favor a more stable 3D structure. von Ragué Schleyer and Pople[34] investigated the reaction of Li_2 with H_2 to produce the rhomboid $(LiH)_2$ dimer at the MP4SDTQ/6-311G** level of theory. Wang and Andrews[32] carried out a more comprehensive IR study of small $(LiH)_n$ clusters (n = 2,3,4) combined with DFT and MP2 vibrational frequencies. Esrafili *et al.*[35] investigated the energetics of various small Li_nH_m ($m \leq n \leq 4$) clusters at the B3LYP level.

Comparatively fewer studies have employed high-level wavefunction methods, such as coupled cluster (CC) theory,[36] on these systems (e.g., see Refs. 21, 37, and 38 for small lithium hydride species, as well as Ref. 39 for an investigation of the larger $Li_{12}H_{12}^-$ and $Li_{12}H_{13}^-$ clusters). Small clusters have even served as benchmarks for emerging quantum computational methods. For instance, recently, Jordan and co-workers[40] showed that hybrid quantum–classical algorithms, such as the variational quantum eigensolver, can be applied to LiH, LiH_2, and LiH_3 to achieve CCSD-quality accuracy. In this small number of studies, the CCSD(T) method is employed. CCSD(T) near the complete basis set (CBS) limit is often considered the "gold standard" of quantum chemistry to treat the electron correlation problem due to its reasonable cost–accuracy trade-off. This method is very successful for well-behaved, moderately sized systems due to a felicitous cancellation of errors between the neglect of higher-order triple excitations and quadruples (see Refs. 41–46). As a result, benchmarking of quantum chemical methods, and more recently the training of machine-learned potentials, are preferentially performed against CCSD(T)/CBS-quality data (e.g., see Refs. 47–52 for some popular databases).

To understand and analyze interatomic interactions, electronic structure, and additivity effects in clusters, it is useful to decompose the total system energy using the many-body expansion (MBE) approach.[53,54] This expresses the total energy as a sum of contributions from 1-, 2-, and 3-body terms, and higher order terms. Up to now, the MBE approach has been successfully applied in hydrogen-bonded or van der Waals-bonded systems,[53–58] which are formed via covalent bonds,[58] metal clusters,[54,59,60] and light nuclei.[61] Previous research has established that the Li–H bond is ionic; thus, we applied the MBE concept to the present systems to analyze their interactions.

In light of the continuing interest in lithium chemistry and the feasibility of high-level electronic structure calculations on larger systems, we have investigated the energetics of small and medium-sized $(LiH)_n$ clusters (n = 2–6) at the CCSD(T)/CBS limit. To the best of our knowledge, the dissociation and total atomization energies (TAE) of these $(LiH)_n$ clusters at their global minima have not yet been examined with sub-kcal/mol accuracy. Beyond providing a new benchmark of energetics, we employ an MBE of the interaction energy of the $(LiH)_n$ clusters to explore the nature of their multicenter bonding. We also characterize the electronic structure of the cyclic species through nucleus-independent chemical shift (NICS) analysis to provide a better understanding of the cooperative effects that dictate cluster stability.

II. COMPUTATIONAL DETAILS

Initial geometries of all $(LiH)_n$ (n = 2–6) clusters were taken from the lowest-energy structures previously identified by Bertolus *et al.*[31] through exhaustive Monte Carlo exploration of the potential energy surface. These global minima and lowest-lying local minima (see Fig. 2 in Ref. 31) were subsequently optimized at the dispersion-corrected B3LYP-D3BJ/def2-TZVPPD level of theory[62–67] using the ORCA v. 6.1.0 program package.[68] For density fitting, we used the auxiliary def2-TZVPPD/C[69] and def2/J[70] basis sets. The chain-of-spheres algorithm[71–73] (RIJCOSX) was also employed along with a large integration grid in DFT (DEFGRID3).[74] Real harmonic frequencies were obtained for all species and the geometries were re-optimized using CCSD/aug-cc-pVTZ[75–78] and MP2/aug-cc-pVQZ.[75–78] To obtain converged energetics, single-point calculations using CCSD and CCSD(T) were carried out using the Dunning correlation-consistent basis sets, aug-cc-pVnZ (n = D,T,Q,5),[75–78] hereafter abbreviated as AVnZ.

All CCSD(T) calculations were carried out using the MOLPRO v. 2022.1 quantum chemical program,[79] and the total electronic CC energies were converged within 10^{-12} E_h. Two separate sets of CC calculations were carried out for all neutral $(LiH)_n$ clusters: (a) valence-only calculations, where the lithium's 1s electrons were kept frozen, and (b) core-valence correlated calculations, where all electrons were correlated. No use of symmetry was made throughout this work. All calculations used conventional CCSD(T) and canonical orbitals, without density fitting as the studied systems are of manageable size for canonical CCSD(T).

Atomic energies were determined using UCCSD(T),[80,81] in which restricted open-shell Hartree–Fock (ROHF) reference orbitals are used for subsequent UCCSD(T) calculations. Atomic charges were obtained from a natural population analysis (NPA)

using the CCSD(T)/AVTZ one-particle density matrix. NPA calculations were performed via the natural bond orbital (NBO)[82] interface implemented in MOLPRO, ensuring that electron correlation effects were included in the population analysis.

To assess the aromaticity of the $(LiH)_n$ clusters, nucleus-independent chemical shift (NICS)[83] values were computed from the isotropic magnetic shielding constants (σ_{iso}) at the CCSD/AVTZ level of theory. These calculations employed the gauge-including atomic orbital[84] (GIAO) method as implemented in Dalton v. 2025.[85] Given that the $(LiH)_n$ clusters lack valence p-electrons, our analysis focused on NICS(0), calculated at the geometric center of the clusters, which is sufficient to capture σ-electron delocalization effects.

To obtain our best estimates for the dissociation energies and total atomization energies of the $(LiH)_n$ clusters, we considered a composite *ab initio* scheme closely related to the Weizmann-2 (W2) protocol developed by Martin and de Oliveira.[86] W2 belongs to the Weizmann-*n* family of *ab initio* composite schemes that achieve sub-kcal/mol accuracy. Here, our approach deviates from the standard W2 theory in three practical respects: (a) we employed two-point basis set extrapolations for the SCF, CCSD, and (T) parts via a AV{Q,5}Z scheme throughout; (b) we used the augmented weighted-core aug-cc-pwCV*n*Z[87] (n = D,T,Q) basis sets for inner-shell correlation; and (c) "small effects," including scalar relativistic effects and the diagonal Born–Oppenheimer corrections[88] (DBOC), were treated according to the HEAT[43–45] protocol.

First, the SCF part was extrapolated separately to the CBS limit using the AVQZ and AV5Z basis sets via Karton and Martin's equation:[89]

$$\Delta E^{\infty}_{SCF} = E_L + (E_L - E_{L-1})/(c-1), \tag{1}$$

$$c = \exp\left(\gamma\left(\sqrt{L} - \sqrt{L-1}\right) - \ln\frac{L+1}{(L-1)+1}\right), \tag{2}$$

where L represents the highest basis set cardinal number (i.e., L = 5 for AV5Z, and $L-1$ = 4 for AVQZ). The γ variable is an effective exponent set to γ = 9.03 for the AV{Q,5}Z extrapolation, as recommended in Table 1 of Ref. 89.

Second, the valence CCSD correlation energy contributions, ΔE^{∞}_{CCSD}, and the parenthetical triples, $\Delta E^{\infty}_{(T)}$, were extrapolated to the CBS limit using the Schwenke[90] formula:

$$\Delta E^{\infty}_{corr.} = E_L + (E_L - E_{L-1}) \Big/ \left[\left(\frac{L}{L-1}\right)^{\alpha} - 1\right], \tag{3}$$

with the extrapolation exponent α set to 3 for the {Q,5} basis set pair, as adopted in W1 and W2 theories.[86] This extrapolation with a fixed extrapolation exponent α = 3 is algebraically equivalent to the two-point extrapolation $A + BL^{-3}$ by Halkier *et al.*,[91] which is used in both Weizmann-*n*[86] and HEAT theories. The frozen-core approximation was applied to keep lithium 1s electrons frozen. Although (T) contributions are known to converge faster than CCSD with respect to the one-particle basis set,[86,90,92] and a downgrade to a (T)/{T,Q} extrapolation would not materially sacrifice accuracy, we used a {Q,5} extrapolation for both CCSD and (T) contributions as the computational cost for the present systems was manageable. Post-CCSD(T) effects were not investigated in the present work.

Third, the core–valence correlation contribution, ΔCV, was computed as the difference between all-electron CCSD(T) and valence-only CCSD(T) contributions to energetics [Eq. (4)]. Both sets of calculations were carried out with the core–valence-weighted correlation-consistent aug-cc-pwCV*n*Z (in short AwCV*n*Z) basis sets.[87] These ΔCV contributions were extrapolated from TZ and QZ basis sets via the Schwenke formula [Eq. (3)] with an extrapolation exponent α set to 3.22 for the CCSD and (T) energy components:[86]

$$\Delta\,\mathrm{CV} = \Delta E_{\mathrm{all-electron,CCSD(T)}} - \Delta E_{frozen-core,CCSD(T)}. \tag{4}$$

Fourth, scalar relativistic effects were accounted for via all-electron CCSD(T) calculations using the "exact two-component" (X2C)[93] approach as implemented in MOLPRO. We chose a mixed basis set combination (denoted a'VQZ), pairing aug-cc-pVQZ for Li with cc-pVQZ for H for the non-relativistic corrections, and used the corresponding recontracted basis sets for the relativistic treatment.[94] Because scalar relativistic effects are highly localized near the atomic core and hydrogen lacks core density, expanding the hydrogen basis set with diffuse functions (AVQZ) did not change the relativistic corrections appreciably (differences $<10^{-6}$ E_h). This relativistic treatment follows the HEAT protocol and recent work by Martin and Sylvetsky,[95] who developed a model based on atomic populations to predict relativistic corrections.

Fifth, the diagonal Born–Oppenheimer[88] corrections (DBOC) were computed at the SCF/AVTZ level to address the limitations of the Born–Oppenheimer approximation. The DBOC terms were obtained using the CFOUR v. 2.1 program package.[96] This treatment is less demanding and less expensive than a correlated treatment at the CCSD level. Indeed, the Hartree–Fock-level DBOC is a standard approximation widely employed in the literature.[41,43–45,86,97–103]

We accounted for the basis-set superposition error (BSSE) in the dissociation energies of $(LiH)_n$ using the standard counterpoise (CP) procedure of Boys and Bernardi.[104] The CP correction for a n-body cluster is defined as

$$\Delta E_{CP} = \sum_i \left(E[LiH]_i - E[LiH]^*_i\right), \tag{5}$$

where $E[LiH]_i$ represents the "raw" energy of the i-th LiH monomer at its frozen cluster geometry computed with its own basis functions, and $E[LiH]^*_i$ is the energy of the same monomer computed in the presence of the "ghost" basis functions of all other monomers.

This rigorous methodology was applied individually to the SCF, CCSD, and (T) components. We note that the CP methodology has been applied for decades, from hydrogen-bonded networks[105] to ionic aggregates.[106] The systematic reduction of BSSE near the CBS limit has recently been exploited by one of us to optimize basis-set extrapolation parameters.[107]

We investigated the multireference (MR) character of the studied species. Several well-known diagnostics of nondynamic correlation were considered, including T_1,[108] D_1,[109–111] and D_2,[109] computed from all-electron CCSD/aug-cc-pwCVTZ calculations. Across all investigated species, T_1 consistently remains below 0.008, far below the standard threshold of 0.02 for closed-shell systems. Similarly, D_1 is uniformly below 0.016 (<0.05), and D_2 does not exceed 0.18. These results rigorously confirm the single-reference, closed-shell nature of the ground states. The complete set of values is provided in the supplementary material.

To verify the spin multiplicity of the ground state, high-spin states were explicitly calculated across all systems. We find that all investigated molecules adopt closed-shell singlet ground states (S_0). The singlet–triplet ($T_1 - S_0$) and singlet–quintuplet ($Q_1 - S_0$) spin-state splittings are all positive and very large; the lowest-lying triplet states remain energetically unfavorable by a hefty 90–105 kcal/mol on average for most species at the B3LYP-D4 level. This energy ordering is preserved for both vertical and adiabatic excitations, where the term adiabatic refers to the fully optimized structures of the respective states. Furthermore, these large spin-state gaps are highly consistent across the DFT, MP2, and CCSD levels of theory. Associated electronic energies are available in the supplementary material.

Finally, to investigate the performance of several widely used density functionals against our CCSD(T)/CBS energetics, we considered five functionals: B3LYP,[66,67] B3LYP-D4,[62,63] ωB97M-D4,[112] M06-2X,[113] and revDSD-PBEP86-D4.[114] The D4 empirical dispersion correction[115,116] was included to accurately account for long-range interactions between the remote LiH groups. All single-point energy DFT calculations at the CCSD/AVTZ-optimized geometries were performed using the def2-QZVPP[64] basis set in ORCA, employing the TightSCF option and the DefGrid3 option for the integration grid. Furthermore, we employed the resolution of identity approximation[117,118] (RI) with the chain-of-spheres algorithm[71–73] (RIJCOSX) along with Weigend's[69] def2/J auxiliary basis set.

III. RESULTS AND DISCUSSION

A. Geometries of $(LiH)_n$ clusters

Figure 1 shows the optimized structures of the $(LiH)_n$ species, which are true minimum structures with real harmonic frequencies. Table I provides selected structural parameters, and the Cartesian geometries of all systems are given in the supplementary material. Starting with the structural properties of the cyclic lithium hydrides, Table I shows their average Li–H bond lengths, Li–H–Li bond angles, and atomic NPA charges. As the ring size increases from $(LiH)_2$ to $(LiH)_5$, the Li–H bond contracts systematically. Concurrently, the average Li–H–Li bond angle systematically opens from 80.6° in $(LiH)_2$ to 131.7° in $(LiH)_5$. The larger the angle, the more efficiently the charge repulsions are minimized, which makes the larger cyclic systems more stable and alleviates the geometric constraints that seem to destabilize smaller clusters. Beyond $(LiH)_2$, the NPA charges on Li and H remain nearly constant (±0.81e). This suggests that the Li–H bond remains ionic and resilient to any changes in cluster structure.

For the LiH diatomic molecule, valence-level CCSD/AVTZ yields a bond length of 1.6104 Å, which slightly contracts to 1.6083 Å upon expansion to the AVQZ basis set. The most accurate result was obtained at the all-electron CCSD(T)/AwCV5Z level, which predicts a bond length of 1.5954 Å, in excellent agreement with the experimental measurement of 1.596 Å.[119] At this same high level, the dissociation energy is 57.92 kcal/mol. While valence CCSD(T) optimizations would likely lead to subtle structural changes (e.g., slight bond contraction), geometry optimizations at the CCSD(T) level become cost-prohibitive for larger systems. As a result, CCSD/AVTZ was chosen as a reliable yet efficient compromise in this work.

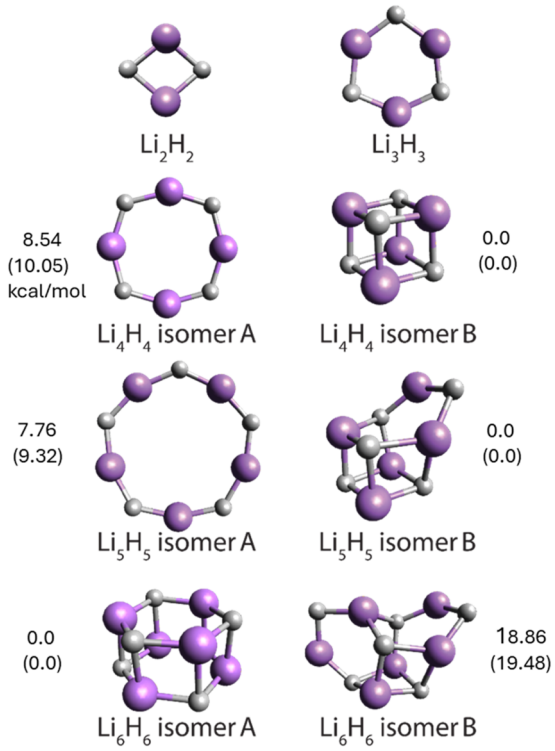

FIG. 1. Optimized structures of the studied $(LiH)_n$ species in this work. Relative energies (in kcal/mol) are shown at the CCSD(T)/aug-cc-pVTZ level of theory (valence electrons are correlated), with values in parentheses indicating the all-electron CCSD(T)/aug-cc-pwCV5Z level (where the 1s electrons of lithium are correlated).

For the dibridged $(LiH)_2$ cluster, CCSD/AVTZ yields Li–Li and H–H distances of 2.285 and 2.695 Å, respectively. These values are in excellent agreement with the D_{2h} structure of $(LiH)_2$ reported by Grein,[38] who obtained Li–Li and H–H distances of 2.2848 and 2.6888 Å, respectively, at the CCSD(T)/AVQZ level. Another direct comparison can be drawn with the 2007 study by Esrafili *et al.*,[35] who investigated various Li_nH_m ($m \le n \le 4$) topologies at the B3LYP/6–311++G(2d,2p) level. The authors reported a shorter Li–Li distance of 2.268 Å for Li_2H_2 using B3LYP. For the larger clusters, three of our structures overlap with those reported in Ref. 35: the cyclic Li_3H_3 cluster and the two Li_4H_4 isomers (cyclic and cubane-like). Once again, our CCSD/AVTZ and CCSD/AVQZ optimized structures systematically exhibit slightly longer bond lengths than their B3LYP ones. Specifically, for the Li–H bond, we obtained CCSD/AVTZ (AVQZ) values of 1.732 (1.730) Å, 1.713 (1.711) Å, and 1.854 (1.851) Å for Li_3H_3 and Li_4H_4 isomers A and B, respectively. In contrast, the published DFT values are 1.71, 1.695, and 1.834 Å, respectively. This discrepancy can be attributed to the inherent limitations of the B3LYP functional—particularly its lack of dispersion corrections and the presence of self-interaction errors—as CCSD provides a more rigorous treatment of dynamic electron correlation.

Comparing our CCSD/AVTZ, CCSD/AVQZ, and MP2/AVQZ geometries, we observe a subtle reduction of all Li–H bonds with

TABLE I. Average bond lengths (Å), bond angles (deg), and NPA charges on lithium (q_{Li}) and hydrogen atoms (q_H).

Species	R_{Li-H}	$\varphi_{Li-H-Li}$	q_{Li}	q_H	R_{Li-H}	R(Li–H)	R(Li–H)
	CCSD/AVTZ				CCSD/AVQZ[b]	MP2/AVQZ[b]	CCSD(T)/AwCV5Z[c]
LiH	1.610		0.845	−0.845	1.608	1.603	1.5954 (1.596)[a]
$(LiH)_2$	1.767	80.6	0.841	−0.841	1.766	1.762	
$(LiH)_3$	1.732	107.6	0.815	−0.814	1.730	1.726	
$(LiH)_4$ A	1.713	122.2	0.809	−0.809	1.711	1.708	
$(LiH)_5$ A	1.704	131.7	0.809	−0.809		1.698	
$(LiH)_4$ B	1.854				1.851	1.846	
$(LiH)_5$ B	1.834					1.826	
$(LiH)_6$ A	1.842					1.834	
$(LiH)_6$ B	1.820					1.813	

[a]Enclosed in parentheses is the experimental value from Ref. 119.
[b]Valence-only calculations where lithium's 1s electrons are kept frozen.
[c]All-electron (AE) calculations, in which all electrons are correlated.

a decrease in the basis set or with the switch from CCSD to MP2 geometries. Comparing CCSD/AVTZ and MP2/AVQZ, focusing only on the primary Li–H bonds (those shorter than 2.5 Å), the mean signed deviation (MSD) is a mere −0.007 Å between the CCSD and MP2 optimized structures. Across the $(LiH)_n$ (n = 1–6) series, the average Li–H bond length is 1.796 Å at the CCSD/AVTZ level (see Fig. 1 above) compared to 1.790 Å at the MP2 level (see Table I and supplementary material). Comparing CCSD/AVTZ, which is an affordable method for the larger species, with CCSD/AVQZ, the Li–H bond lengths differ by 0.001 Å for $(LiH)_2$, 0.002 Å for $(LiH)_3$, 0.002 Å for $(LiH)_4$ (isomer A), and 0.002 Å for the compact $(LiH)_4$ (isomer B). Such negligible differences do not materially impact our high-level estimates of energetics. Thus, given that CCSD/AVQZ geometry optimization was not affordable, either MP2/AVQZ or CCSD/AVTZ geometries can be applied for the calculation of the $(LiH)_6$ clusters.

Furthermore, we investigated the impact of the underlying geometry—MP2/AVQZ vs CCSD/AVTZ—on the final energetics. For TAEs, the valence CCSD(T)/AVQZ results show a negligible MSD of 0.002 kcal/mol between the two geometry sets. Similarly, while the dissociation energies relative to the LiH monomers are slightly underestimated using MP2 geometries (MSD = −0.065 kcal/mol), both levels of theory provide a sufficiently accurate foundation for attaining chemical accuracy in subsequent high-level energy calculations.

Finally, the average Li–H bond distances of the calculated minima that are polycyclic structures, that is, cubane, range from 1.813 to 1.854 Å, and they are about 0.14 Å longer than those of the corresponding monocyclic ones. The reason for this elongation is that all or some of the atoms form three bonds instead of two, as is the case with cyclic structures.

B. Dissociation energies

Table II reports the dissociation energies of the $(LiH)_n$ clusters. We define the dissociation energy relative to LiH monomers (ΔE_{LiH}) as the energy released when the cluster dissociates into n LiH monomers, thereby capturing cooperative binding effects beyond the monomer level:

$$\Delta E_{LiH} = n\ E(\mathrm{LiH}) - E\big((\mathrm{LiH})_n\big). \tag{6}$$

The total electronic energy is partitioned into its constituent parts: the SCF energy, valence correlation [CCSD and (T)], core–valence corrections (ΔCV), scalar relativistic effects, and the DBOC. Furthermore, the BSSE corrections from full CP-corrected calculations are also shown, and they were computed via the Boys and Bernardi's[104] scheme.

All studied clusters are bound relative to their monomer units and constituent atoms, exhibiting positive dissociation energies. The SCF part accounts for the largest absolute fraction of the binding energy and increases systematically with system size. However, while SCF captures most of the interaction, electron correlation still plays a major role in thermochemistry and structural properties [see Fig. 2(a)]. This can be observed when comparing the cyclic and compact isomers of $(LiH)_n$. For example, for n = 5, there seems to be no major energetic difference between compact and open cyclic isomers at the SCF/CBS limit. Conversely, the valence correlation contributions [CCSD+(T)] favor the compact isomer by ~8.4 kcal/mol, completely reversing this artificial stability at the SCF level. This confirms that many-body electron correlation effects are critical for these interactions.

The valence triples (T) follow a similar trend to the CCSD components. While smaller in absolute magnitude, these higher-order correlation terms scale from 0.35 kcal/mol in $(LiH)_2$ to 2.4 kcal/mol for the compact $(LiH)_6$ isomer A. Once again, the compact isomers have significantly larger (T) contributions, which are roughly three times larger than their cyclic analogues for n = 4 and 5.

Valence BSSE corrections are reported at the AV5Z basis set. All single-basis-set BSSE corrections reduce the dissociation energies, as expected. Although the extrapolated {Q,5} values are tiny, they lack monotonic convergence to the asymptotic BSSE limit, which is an artifact of extrapolating near-zero values. The AV5Z BSSE corrections remain near the CBS limit and are uniformly small

TABLE II. Dissociation energies into individual monomers, ΔE_{LiH},[a] and dissociation energy contributions (in kcal/mol) at the CCSD(T)/CBS level of theory, including core–valence corrections (ΔCV), scalar relativistic effects, and the DBOC.[b]

Contributions to dissociation energy of $(LiH)_n$ clusters relative to free LiH monomers														
					BSSE correction					BSSE correction				
		ΔE^{∞}_{SCF}	ΔE^{∞}_{CCSD}[c]	$\Delta E^{\infty}_{(T)}$[d]	ΔE^{∞}_{SCF}	ΔE^{∞}_{CCSD}[d]	$\Delta E^{\infty}_{(T)}$[d]	ΔCV_{CCSD}[e]	$\Delta CV_{(T)}$[e]	ΔCV_{CCSD}[e]	$\Delta CV_{(T)}$[e]	ΔE_{rel}	ΔE_{DBOC}	ΔE_{total}
Species	isomer	AV{Q,5}Z			AV5Z			AwCV{T,Q}Z		AwCVQZ				
$(LiH)_2$		47.173	1.047	0.345	−0.002	−0.018	0.000	0.702	0.041	−0.021	−0.001	−0.002	−0.017	49.25
$(LiH)_3$		94.045	1.280	0.517	−0.003	−0.032	0.000	1.145	0.067	−0.035	−0.001	−0.002	−0.025	96.96
$(LiH)_4$	A	135.526	1.066	0.586	−0.006	−0.046	0.000	1.509	0.085	−0.050	−0.001	−0.002	−0.036	138.63
$(LiH)_4$	B	137.462	7.264	1.628	−0.006	−0.064	0.000	2.357	0.172	−0.085	−0.002	−0.005	−0.043	148.68
$(LiH)_5$	A	174.456	0.807	0.632	−0.008	−0.059	0.000	1.842	0.102	−0.065	−0.002	−0.002	−0.048	177.65
$(LiH)_5$	B	174.403	8.001	1.876	−0.008	−0.078	0.000	2.749	0.197	−0.103	−0.003	−0.006	−0.056	186.97
$(LiH)_6$	A	227.758	10.463	2.404	−0.017	−0.051	0.000	3.542	0.256	−0.188	−0.002	−0.008	−0.076	244.08
$(LiH)_6$	B	210.334	9.037	2.178	−0.014	−0.106	0.000	3.153	0.224	−0.125	−0.002	−0.007	−0.070	224.60

[a] $\Delta E_{\mathrm{LiH}} = n\ E(\mathrm{LiH}) - E\big((\mathrm{LiH})_n\big)$.
[b] All geometries were optimized at the CCSD/AVTZ level and were used in all subsequent coupled-cluster calculations.
[c] The valence CCSD contribution is defined as the CCSD–SCF difference.
[d] The valence (T) contribution is defined as the CCSD(T)–CCSD difference.
[e] The core–valence correlation contributions, ΔCV_{CCSD} and $\Delta CV_{(T)}$, are defined as the difference between all-electron (AE) and frozen-core (FC) calculations at the CCSD and perturbative triples (T) levels, respectively.

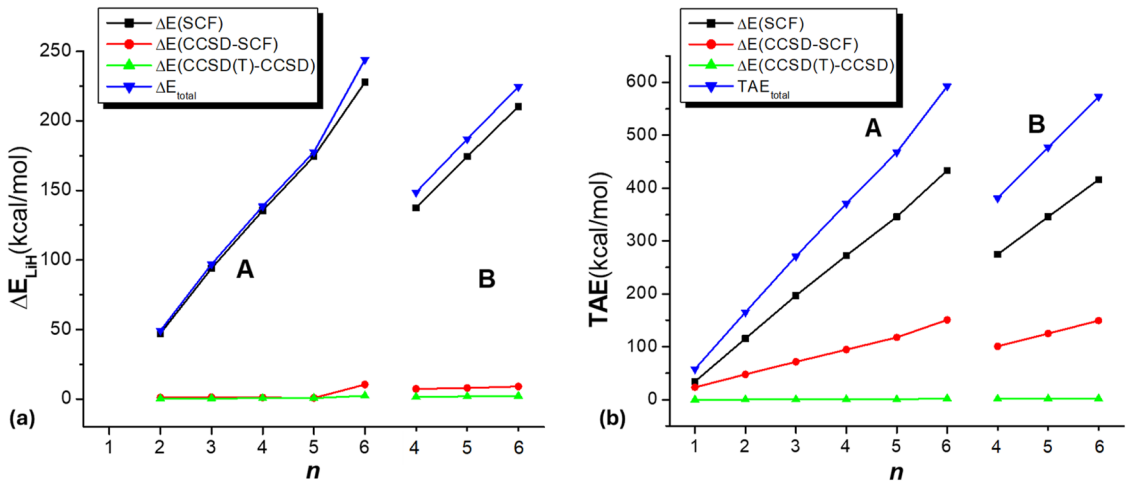

FIG. 2. (a) Total dissociation energy ΔE_{LiH} and dissociation energy contributions with respect to the LiH monomers, and (b) total atomization energies (TAEs) and their energy contributions for $(LiH)_n$ clusters with respect to n at the CCSD(T)/CBS level of theory.

(<0.1 kcal/mol), confirming that residual basis-set incompleteness does not affect the observed trends. In larger clusters, the CCSD BSSE is an order of magnitude larger than the SCF BSSE. Finally, the valence (T) contribution is zero for the isolated monomers, as CCSD is exact for a two-valence-electron system like LiH. Therefore, the associated BSSE correction is also zero.

The core–valence correlation contribution (ΔCV) adds more stability. This is more noticeable at the valence CCSD level than for (T). These values, extrapolated from AwCVTZ and AwCVQZ, increase systematically with cluster size. The largest contributions are 3.54 kcal/mol for ΔCV_{CCSD} and 0.26 kcal/mol for $\Delta CV_{(T)}$ $(LiH)_6$ isomer A. Cyclic isomers have smaller CV contributions than compact species. While the BSSE corrections to ΔCV are destabilizing, they remain small for CCSD and are minuscule for (T) (up to −0.003 kcal/mol). Note that all-electron (T) contributions are not zero now.

The relativistic contributions are also destabilizing and very small, not exceeding 0.01 kcal/mol among the studied clusters. What is more important is the DBOC, which is an order of magnitude larger than the relativistic contributions. This suggests that nuclear

motion effects are more critical than relativistic effects for these light-element species.

C. Total atomization energies (TAEs)

While dissociation energies provide insight into the cooperative effects of cluster formation, the total atomization energies (TAE) reported in Table III offer the definitive measure of thermodynamic stability across the $(LiH)_n$ series. Moving from ΔE_{LiH} to TAE shifts the focus from inter-monomer interactions to the total energy required to fragment the cluster into its constituent atoms:

$$\mathrm{TAE} = n\ E(\mathrm{Li}) + n\ E(\mathrm{H}) - E\big((\mathrm{LiH})_n\big). \tag{7}$$

TAEs are widely used to establish rigorous benchmarks for validating quantum chemical methods (e.g., see Refs. 41, 98, and 120–124) and underpin high-accuracy thermochemical datasets, such as the W4-11 and W4-17 sets.[125,126] Here, our TAEs represent "the bottom of the well" and do not include zero-point vibrational energy (ZPVE) corrections. In addition, the TAEs provide a larger energetic reservoir than ΔE_{LiH}, ranging from 58 kcal/mol for LiH to 573 kcal/mol for the largest lithium hydride cluster studied. Our best estimate for LiH (58.02 kcal/mol) represents its bond dissociation energy and agrees with the experimental value of 58.57 ± 4.6 kcal/mol.[127]

The SCF component contributes the most to the TAE, but the electron correlation is now more important compared with dissociation to LiH monomers. For most $(LiH)_n$ clusters, the valence CCSD term accounts for ~25% of the TAE, and even 40% for LiH. In contrast, the CCSD contribution is less than 5% for ΔE_{LiH} among $(LiH)_n$ clusters, see Fig. 2(b). Note that the TAEs and their energy contributions for the $(LiH)_n$ clusters scale linearly for both the cyclic A structures [apart from $(LiH)_6$ where two bonded six-membered rings are formed] and the B structures.

Because triple excitations describe the correlation of three or more electrons, the (T) term is identically zero for the valence-only treatment of the LiH monomer and constituent atoms. The (T) contributions in Tables II and III are thus equivalent, representing the electron correlation effects that emerge upon cluster formation.

The stabilization of the compact isomers is also evident for TAEs, much like that in the dissociation analysis. This stabilization is attributed primarily to the valence CCSD correlation and the all-electron ΔCV_{CCSD} contribution. For instance, as seen from our best estimates of TAEs, the cubane-like $(LiH)_4$ (isomer B) and compact $(LiH)_5$ are more stable than their cyclic counterparts by 10.1 and 9.4 kcal/mol, respectively. The TAEs confirm that the preference for compact over cyclic architecture is driven not only by the monomer–monomer arrangement but also by electron correlation effects.

D. DFT study

To benchmark the performance of several broadly used DFT methods against our CCSD(T)/CBS data, we considered the standard B3LYP and M06-2X functionals, and three dispersion-corrected functionals: B3LYP-D4, ωB97M-D4, and revDSD-PBEP86-D4. Table IV lists the corresponding error statistics using the def2-QZVPP orbital basis set throughout.

Among the tested methods, the revDSD-PBEP86-D4 double-hybrid functional, which was presented by the Martin group, performs the best with the lowest root-mean-square deviation (RMSD) of 0.37 kcal/mol and a mean signed deviation (MSD) of 0.25 kcal/mol for the small set of molecules at hand. This minimally empirical functional was trained on the chemically diverse GMTKN55 database,[47] and the absolute errors remain less than 1 kcal/mol for all investigated systems, which further confirms that revDSD-PBEP86-D4 remains a very robust option for light-element thermochemistry of well-behaved systems.

TABLE III. Total atomization energies (TAEs)[a] and energy contributions (in kcal/mol) of lithium hydride clusters at the CCSD(T)/CBS level of theory including core–valence corrections (ΔCV), scalar relativistic effects, and the DBOC.[b]

		ΔE^{∞}_{SCF}	ΔE^{∞}_{CCSD}[c]	$\Delta E^{\infty}_{(T)}$[d]	ΔCV_{CCSD}[e]	$\Delta CV_{(T)}$[e]	ΔE_{rel}	ΔE_{DBOC}	TAE_{total}
Species	isomer		AV{Q,5}Z			AwCV{T,Q}Z			
LiH		34.282	23.406	0.000	0.257	0.083	−0.001	−0.005	58.02
$(LiH)_2$		115.738	47.859	0.345	1.216	0.206	−0.005	−0.026	165.33
$(LiH)_3$		196.892	71.497	0.517	1.916	0.315	−0.006	−0.039	271.09
$(LiH)_4$	A	272.654	94.689	0.586	2.536	0.416	−0.008	−0.055	370.82
$(LiH)_4$	B	274.591	100.886	1.628	3.385	0.502	−0.011	−0.062	380.92
$(LiH)_5$	A	345.866	117.836	0.632	3.126	0.515	−0.010	−0.072	467.89
$(LiH)_5$	B	345.814	125.029	1.876	4.033	0.610	−0.013	−0.079	477.27
$(LiH)_6$	A	433.451	150.896	2.404	5.084	0.751	−0.016	−0.104	592.47
$(LiH)_6$	B	416.027	149.471	2.178	4.694	0.720	−0.015	−0.098	572.98

[a] $\mathrm{TAE} = n\ E(\mathrm{Li}) + n\ E(\mathrm{H}) - E\big((\mathrm{LiH})_n\big)$.
[b] All geometries were optimized at the CCSD/AVTZ level and were used in all subsequent coupled-cluster calculations.
[c] The valence CCSD contribution is defined as the CCSD–SCF difference.
[d] The valence (T) contribution is defined as the CCSD(T)–CCSD difference.
[e] The core–valence correlation contributions, ΔCV_{CCSD} and $\Delta CV_{(T)}$, are defined as the difference between all-electron (AE) and frozen-core (FC) calculations at the CCSD and perturbative triples (T) levels, respectively.

TABLE IV. Dissociation energies, ΔE_{LiH},[a] in kcal/mol with various DFT functionals using the def2-QZVPP basis set and error statistics with respect to the CBS values.[b]

Species	Isomer	B3LYP	B3LYP-D4	ωB97M-D4	M06-2X	revDSD-PBEP86-D4	CCSD(T)/CBS[b]
$(LiH)_2$		48.08	49.27	48.16	50.00	49.50	49.25
$(LiH)_3$		95.21	96.43	94.91	97.95	97.15	96.96
$(LiH)_4$	A	136.63	138.43	136.01	139.22	139.09	138.63
$(LiH)_4$	B	143.10	145.96	145.46	152.87	148.40	148.68
$(LiH)_5$	A	175.49	177.74	174.47	177.27	178.35	177.65
$(LiH)_5$	B	180.46	184.46	183.38	191.68	187.03	186.97
$(LiH)_6$	A	235.55	241.08	239.32	250.28	244.29	244.08
$(LiH)_6$	B	216.95	222.19	220.74	230.00	225.04	224.60
	RMSD	5.22	1.90	3.22	3.70	0.37	
	MSD	−4.42	−1.41	−3.05	2.81	0.25	

[a] $\Delta E_{LiH} = n\ E(LiH) - E\left((LiH)_n\right)$.
[b] Best estimate: CCSD(T)/CBS values, that is, ΔE_{total} values in Table II.

In contrast, the standard B3LYP functional significantly underbinds with an RMSD of 5.22 kcal/mol and an MSD of −4.42 kcal/mol. This error increases rapidly with increasing system size, reaching −8.53 kcal/mol for the compact Li_6H_6 (isomer A). However, the inclusion of the D4 empirical dispersion correction (B3LYP-D4) cuts the RMSD in half, with deviations below 3 kcal/mol. Clearly, the dispersion correction accounts for the long-range interactions of the LiH units. Both ωB97M-D4 and M06-2X offer intermediate accuracy between standard B3LYP and the top performer revDSD-PBEP86-D4.

The binding energy per atom is defined as the total atomization energy (TAE) of the whole cluster divided by the total number of atoms comprising it. The DFT and CCSD(T)/CBS average binding energies per atom are given in Table V; previously published B3LYP/6–311++G(2d,2p) data[35] are in good agreement, despite minor differences in geometries.

The average dissociation energy per LiH unit ($\Delta E_{LiH}/n$) of $(LiH)_n$ clusters is plotted as a function of cluster size in Fig. 3, which compares the MP2, CCSD, CCSD(T) and DFT results with our best estimated values. For the monocyclic structures, all methodologies provide good results. However, for the polycyclic species, the inclusion of core–valence correlation, scalar relativistic effects, and DBOC is needed for accurate energetic predictions at the CCSD level and further improves the CCSD(T) results. Notably, the accuracy of the MP2 data is comparable to that of RCCSD(T). In general, DFT performs well and the errors are in a tight range. In Fig. 3(d), M06-2X overestimates the $\Delta E_{LiH}/n$ values, while B3LYP underestimates them. Among the tested functionals, revDSD-PBEP86-D4 provides the best results, even better than the single-basis-set (one-shot) CCSD(T), showing an excellent agreement with our best CCSD(T)/CBS values.

The average total atomization energy (TAE/2n) of $(LiH)_n$ clusters as a function of cluster size is shown in Fig. 4, comparing the MP2, CCSD, CCSD(T), and DFT levels against our reference CCSD(T)/CBS data. For both monocyclic and polycyclic structures, the CCSD and CCSD(T)/AwCV5Z results are in excellent agreement with the CCSD(T)/CBS reference. While the AwCVDZ basis set underestimates the TAE/2n values, the AVQZ and AV5Z basis

TABLE V. Calculated average binding energies per atom[a] in kcal/mol of $(LiH)_n$ clusters.

	Isomer	B3LYP[b]	B3LYP	B3LYP-D4	ωB97M-D4	M06-2X	revDSD-PBEP86-D4	CCSD(T)/CBS[c]
LiH		29.64	29.21	29.43	29.95	28.30	28.36	29.01
$(LiH)_2$		41.72	41.24	41.75	41.99	40.80	40.73	41.33
$(LiH)_3$		45.58	45.08	45.50	45.77	44.63	44.55	45.18
$(LiH)_4$	A	46.79	46.29	46.73	46.95	45.71	45.74	46.35
$(LiH)_4$	B	47.63	47.10	47.68	48.14	47.41	46.91	47.61
$(LiH)_5$	A		46.76	47.21	47.40	46.03	46.19	46.79
$(LiH)_5$	B		47.26	47.88	48.29	47.47	47.06	47.73
$(LiH)_6$	A		48.84	49.52	49.90	49.16	48.71	49.37
$(LiH)_6$	B		47.29	47.95	48.35	47.47	47.11	47.75

[a] TAE/2n.
[b] B3LYP/6–311++G(2d,2p) values sourced from Ref. 35.
[c] Best estimate: CCSD(T)/CBS values scaled by the number of atoms, that is, $TAE_{total}/2n$ values in Table III.

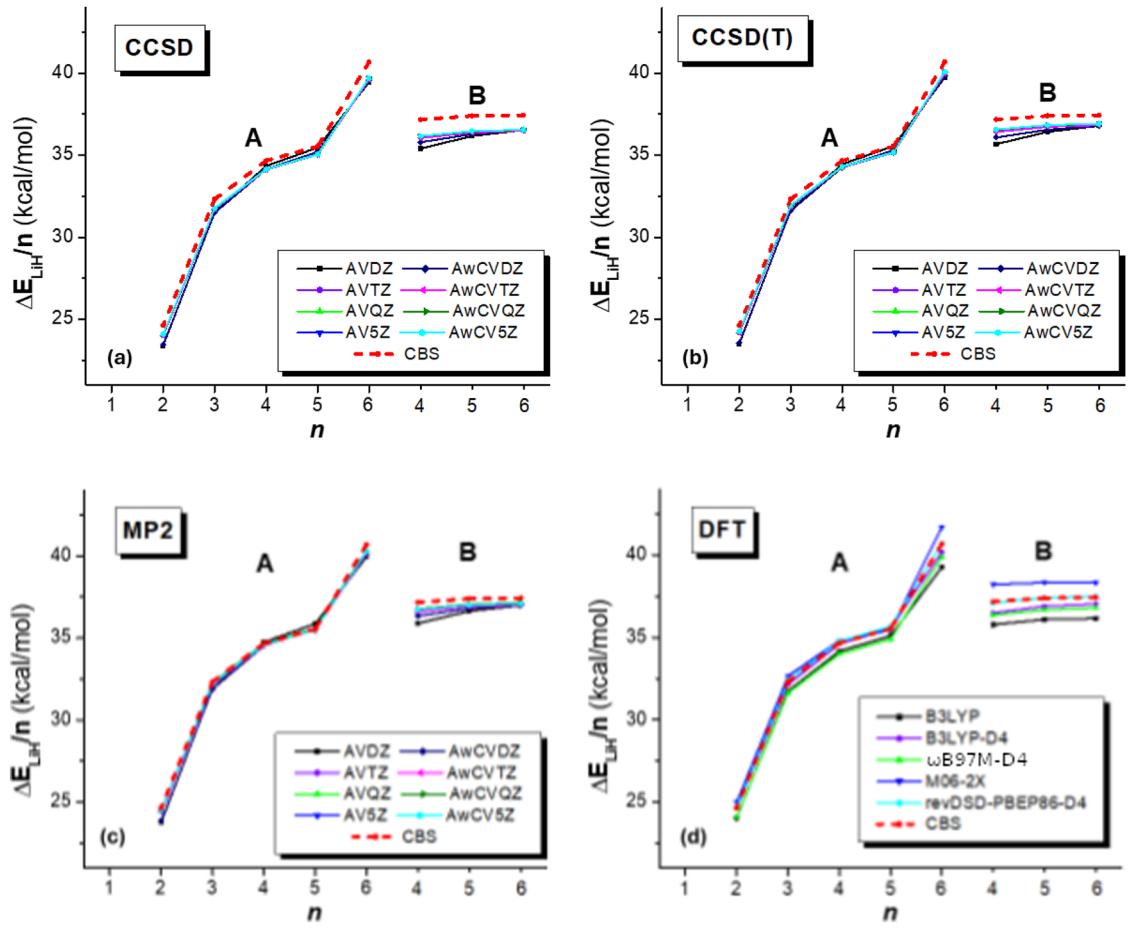

FIG. 3. Average dissociation energy per LiH unit ($\Delta E_{LiH}/n$) for $(LiH)_n$ clusters as a function of cluster size n (all values are in kcal/mol). Results are shown for (a) CCSD, (b) CCSD(T), (c) MP2 using Dunning's basis sets, and (d) several DFT functionals using the def2-QZVPP basis set. Data for both monocyclic (A) and polycyclic (B) isomers are shown. The dashed red lines represent our best CCSD(T)/CBS estimates, which include core-valence correlation, scalar relativistic effects, and the diagonal Born–Oppenheimer correction.

sets overestimate them. On the contrary, the MP2 method overestimates the TAE/2n values; specifically, the AVQZ and AV5Z basis sets provide the most accurate MP2 data, whereas the weighted-core basis sets provide systematically lower values. Interestingly, the selected DFT functionals perform very well, with B3LYP providing that the best agreement with our best CBS values.

Regarding the monocyclic structures, the $\Delta E_{LIH}/n$ and TAE/2n values seem converged. By fitting these values to an exponential function ($y = y_0 + ae^{-x/b}$, see Fig. 5), we obtained extrapolated limits of 35.85 and 46.93 kcal/mol, respectively. Note that for $(LiH)_n$ clusters with $n > 6$, monocyclic rings are only local minima because the polycyclic structures become more energetically stable. It should be noted that the average atomization energy of the LiH molecule is only 29.01 kcal/mol; thus, the formation of the cyclic cluster increases the TAE/2n by 62%.

We also examined how correlation-consistent basis sets perform in DFT calculations of lithium hydride energetics. Because the basis set convergence of DFT for thermochemistry is well established—with both large-sized def2-type basis sets and correlation-consistent basis sets known to converge to the CBS limit (e.g., see Refs. 128 and 129 and Tables II–V in Ref. 130)—our original choice of def2-type basis sets was well justified. Nonetheless, to address this concern, we considered the cc-pVnZ and cc-pwCVnZ (n = D,T,Q) basis sets in all single-point energy calculations at the CCSD/AVTZ-optimized geometries of the lithium hydrides. The corresponding RMSD values for the dissociation energies are reported in Table VI.

Overall, we find that the errors in DFT are largely insensitive to the basis set choice. Expanding the basis set to def2-QZVPP and cc-pwCVQZ yields nearly the same RMSDs across the tested methods, such as 0.37 and 0.41 kcal/mol for revDSD-PBEP86-D4, respectively. Upgrading to the largest cc-pwCV5Z basis sets leads to comparable performance to def2-QZVP for B3LYP, B3LYP-D4 and revDSD-PBEP86-D4, although ωB97M-D4 and M06-2X calculations with this basis set did not converge due to linear dependency issues. In addition, the standard cc-pVnZ basis sets give similar results to those

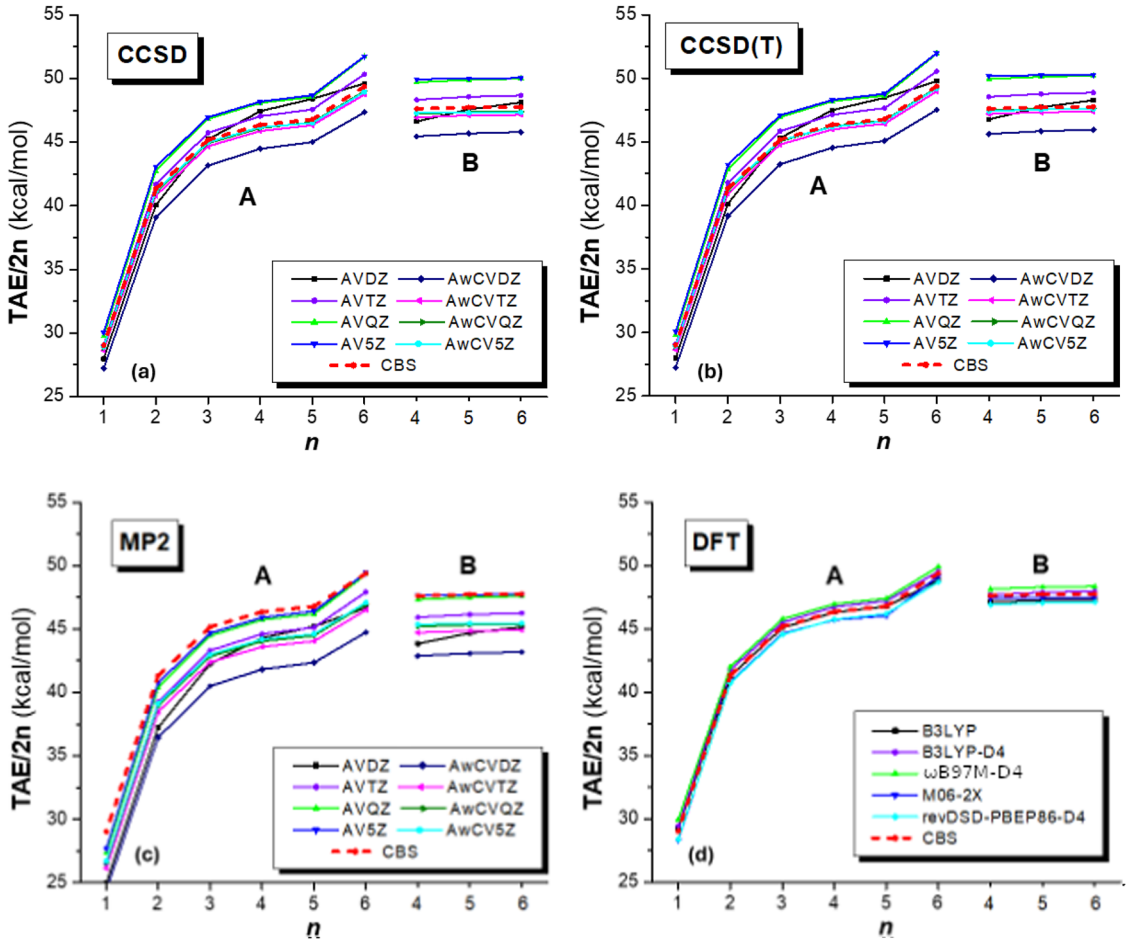

FIG. 4. Average total atomization energies (TAE) per atom (TAE/2*n*) for $(LiH)_n$ clusters as a function of cluster size *n* (all values are in kcal/mol). Results are shown for (a) CCSD, (b) CCSD(T), (c) MP2 using Dunning's basis sets, and (d) several DFT functionals using the def2-QZVPP basis set. Data for both monocyclic (A) and polycyclic (B) isomers are shown. The dashed red lines represent our best CCSD(T)/CBS estimates, which include core–valence correlation, scalar relativistic effects, and the diagonal Born–Oppenheimer correction.

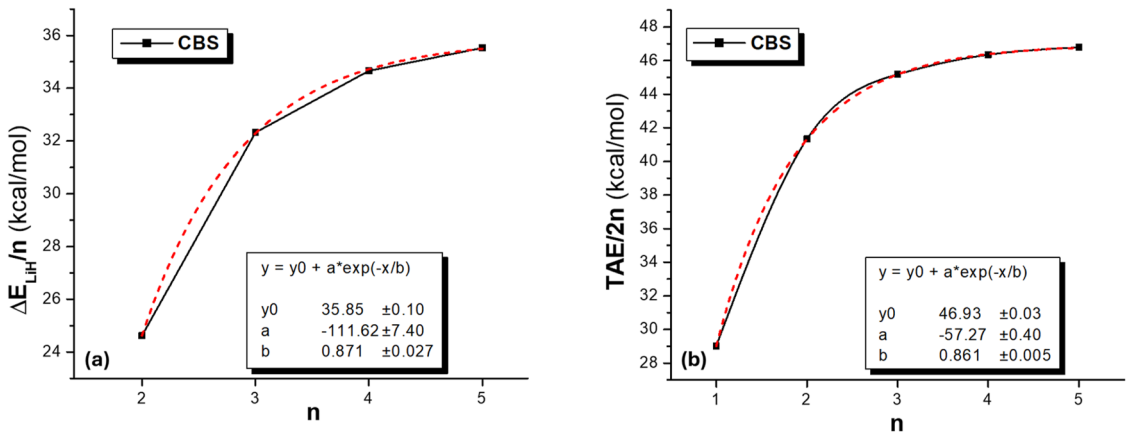

FIG. 5. Exponential extrapolation to the cluster limit for (a) the average dissociation energy per LiH unit ($\Delta E_{LiH}/n$) of $(LiH)_n$ clusters and (b) the average atomization energy per atom (TAE/2*n*). The black squares represent our high-level CCSD(T)/CBS data, while the dashed red lines indicate the exponential fit ($y = y_0 + ae^{-x/b}$). The reference values also include core–valence correlation, scalar relativistic effects, and the diagonal Born–Oppenheimer correction.

TABLE VI. RMSD (in kcal/mol) of dissociation energies for lithium hydride clusters using various DFT methods and orbital basis sets relative to our CCSD(T)/CBS best estimates.

Basis set	B3LYP	B3LYP-D4	ωB97M-D4	M06-2X	revDSD-PBEP86-D4
def2-TZVPP	5.66	2.34	3.72	2.99	1.30
def2-QZVPP	5.22	1.90	3.22	3.70	0.37
cc-pwCVTZ	5.07	1.75	2.85	3.83	0.41
cc-pwCVQZ	5.00	1.69	3.16	3.45	0.35
cc-pwCV5Z	5.02	1.70	n/a	n/a	0.41
cc-pVTZ	4.52	1.39	2.15	4.22	2.73
cc-pVQZ	4.24	1.09	2.65	4.20	6.52
cc-pV5Z	5.03	1.71	3.27	3.77	6.17

obtained with def2-QZVPP; for example, ωB97M-D4 yields RMSD values of 3.27 and 3.22 kcal/mol for cc-pV5Z and def2-QZVPP, respectively.

However, some discrepancies arise for revDSD-PBEP86-D4 with the cc-pV*n*Z basis sets, resulting in very large RMSD values (6 kcal/mol). This discrepancy occurs in the MP2 component of the double hybrid, which has not converged with cc-pV*n*Z and could be attributed to the lack of core-polarization functions. The issue is resolved with the cc-pwCV*n*Z family, which provides the necessary radial flexibility and solves this problem. Individual dissociation energies are given in the supplementary material.

E. Many-body expansion of the interaction energy

The total interaction energy (ΔE_{int}) of the $(\text{LiH})_n$ clusters, which are the negative values of the dissociation energies, can be partitioned using the MBE. This formalism expresses the total energy as a sum of interactions among all constituent monomers, dimers, trimers, and higher-order subsystems.[40,53–55] Beyond providing physical insight into the interactions within the molecular cluster, the MBE facilitates calculations by allowing massive parallelization. Moreover, it offers a pathway for truncating the expansion, enabling the use of higher-accuracy wavefunction methods on otherwise inaccessible systems.

While initially applied to water clusters,[40,53–57] the MBE has since been extended to a variety of systems, including hydrogen-bonded systems,[131] ion-water systems,[132–135] covalent molecular systems,[58] metal clusters,[54,59,60] and light nuclei.[61] Here, we apply the MBE to clusters where the "body" is a LiH unit held together by ionic bonds. The formalism of the MBE expansion is given below:

$$\Delta \text{E}_{\text{int}} = E(123\,456) - \sum_{i=1}^{6} E\left(X_i^{gs}\right) \approx \Delta E(1-B) + \Delta E(2-B) + \Delta E(3-B) + \Delta E(4-B) + \Delta E(5-B) + \Delta \text{E}(6-\text{B}), \quad (8)$$

$$\Delta E(1-B) = \sum_{i}^{6} \left[E(X_i) - E\left(X_i^{gs}\right)\right], \quad (9)$$

$$\Delta E(2-B) = \sum_{i<j}^{6} \Delta^2 E_{ij}, \quad (10)$$

$$\Delta^2 E_{ij} = E(X_i X_j) - E(X_i) - E(X_j), \quad (11)$$

$$\Delta E(3-B) = \sum_{i<j<k}^{6} \Delta^3 E_{ijk}, \quad (12)$$

$$\Delta^3 E_{ijK} = E\left(X_i X_j X_k\right) - E(X_i) - E\left(X_j\right) - E(X_k) - \Delta^2 E_{ij} - \Delta^2 E_{ik} - \Delta^2 E_{jk}. \quad (13)$$

Figure 6(a) depicts the MBE contributions to the interaction energies of the monocyclic $(\text{LiH})_n$ clusters and the polycyclic $(\text{LiH})_6$ cluster (isomer A). In this analysis, each "body" is defined as an LiH molecule, and all MBE calculations were carried out at the MP2/AVQZ level. The two-body (2-B) contributions, which represent the sum of pairwise interactions, provide most of the stabilization—which is not surprising, given the ionic nature of the interaction—and they scale with system size. Furthermore, for the polycyclic $(\text{LiH})_6$ (isomer A), the 2-B term is larger than the $\Delta \text{E}_{\text{LiH}}$ value (see Table VII).

The three-body (3-B) terms further stabilize the clusters, contributing −6.23, −15.28, −22.87, and −49.53 kcal/mol, for n = 3 through 6, respectively (see Table VII). Stabilization due to the 2-B and 3-B terms results from the strong charge separation in LiH (see below). While the 4-B and 5-B terms are very small for the smaller monocyclic $(\text{LiH})_4$ and $(\text{LiH})_5$ rings, the expansion for the compact $(\text{LiH})_6$ gives a distinct pattern: the 4-B term is destabilizing, while the 5-B term stabilizes it. Interestingly, the destabilizing 4-B contribution exceeds the 3-B term, which strongly suggests that higher-order interactions play a major role in the energetics of polycyclic species. Finally, the 1-B term corresponds to the relaxation of the LiH monomers, it is about 3 kcal/mol for the monocyclic structures; however, for the polycyclic $(\text{LiH})_6$ isomer A, the relaxation is significant at 14.41 kcal/mol. This means that significant geometric distortion is required to form cage-like structures. Nevertheless, it should be noted that the 2-B term remains larger than the $\Delta \text{E}_{\text{LiH}}$ value.

Figure 6(b) depicts the MBE contributions to the interaction energies of the monocyclic $(\text{LiH})_2$ and $(\text{LiH})_3$ clusters using an atomic decomposition, where each "body" is an individual Li or H atom. Because the atoms are considered in their electronic ground state, the 1-B term is zero by definition. The 2-B term dominates

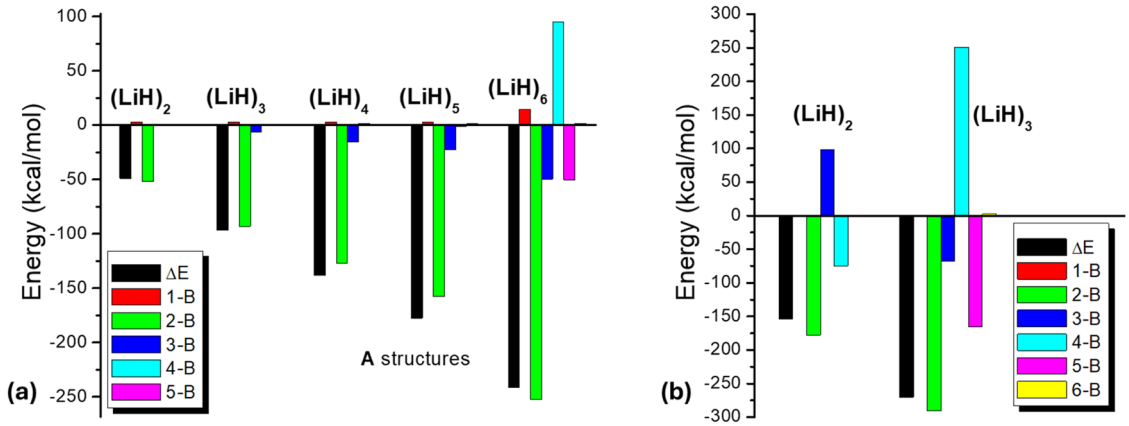

FIG. 6. MBE contributions to dissociation energies of cyclic $(LiH)_n$ (a) with respect to LiH molecules and (b) with respect to lithium and hydrogen atoms.

TABLE VII. MBE analysis of the interaction energies of cyclic $(LiH)_n$ with respect to LiH molecules in kcal/mol at MP2/AVQZ.

Cluster	1-B	2-B	3-B	4-B	5-B	6-B	ΔE_{LiH}
Li_2H_2	2.97	−51.92					−48.95
Li_3H_3	2.77	−93.13	−6.23				−96.59
Li_4H_4 (A)	2.96	−127.33	−15.28	1.30			−138.35
Li_5H_5 (A)	2.68	−157.91	−22.87	−1.04	1.66		−177.48
Li_6H_6 (A)	14.41	−252.48	−49.53	94.77	−50.33	1.66	−241.50

the total interaction energy, while the higher-order terms oscillate between stabilizing and destabilizing, as typically observed in similar expansions.[54]

F. BSSE convergence with valence basis sets

It is interesting to evaluate the BSSE effect in the present benchmarking calculations. A well-known pitfall in all-electron calculations that can lead to catastrophic errors is the omission of weighted core functions. Hargittai and Varga[136] provided a cautionary example when they discovered large discrepancies in the bond lengths of aluminum monohalides when standard valence correlation basis sets (cc-pVnZ) were used instead of the appropriate cc-pwCVnZ for MP2 and CCSD(T) calculations. Tzeli and Tsekouras[137] further demonstrated the unreliable nature of the approach, noting a massive overestimation of the BSSE correction, by as much as 10 kcal/mol, for the interaction energy of the benzene–Na^+ complex at the all-electron MP2/AVTZ level of theory. This phenomenon occurs because valence basis sets lack the tight functions necessary to properly describe inner-core correlation.

Here, we find that the size of the BSSE is heavily dependent on the inclusion of core-correlation functions (see Table VIII). As highlighted in Ref. 137, correlating core electrons with valence-only basis sets leads to spurious conclusions and an artificial overestimation of binding energies due to massive BSSE. This is strikingly evident in the non-monotonic convergence of our CCSD/AVnZ results. For example, the CCSD BSSE correction for $(LiH)_2$ actually widens from −2.499 kcal/mol to −4.134 kcal/mol when moving from AVTZ to AVQZ. This error spirals into a catastrophe for larger clusters, where we find a staggering 25 kcal/mol BSSE for $(LiH)_6$. So, even though Li is a light atom, the BSSE correction should be considered at the CCSD level when the basis set used is not a weighted core basis set.

Interestingly, the parenthetical triples (T) appear relatively immune to this issue (see the lower section of Table VIII). This stability likely stems from its dependence on the converged CCSD amplitudes, which makes the (T) correction less sensitive to the core-region structure. The most reliable remedy is to use the weighted core basis sets (AwCVnZ), which yield the expected systematic decrease in BSSE as the basis set size increases. With the AwCVQZ basis set, the CCSD BSSE corrections now range from −0.059 to −0.353 kcal/mol, while the (T) component of the BSSE remains below 0.005 kcal/mol across the entire series.

G. Bonding analysis

Intrinsic bond orbital (IBO) analysis was performed following the localization scheme developed by Knizia,[138] in which the orbitals are constructed by localizing the occupied MOs such that their electron density is maximally concentrated on a minimal set of atoms. These calculations were carried out at the PBE/def2-TZVPP level[64,139,140] (as recommended in Ref. 138) using the dedicated IBO analysis program IBBA implemented in MOLPRO. Wiberg[141] bond orders were computed, and DFT partial atomic charges were obtained from the charge composition analysis using IBBA.

Starting with the LiH diatomic, we observe a 2-center, 2-electron (2c–2e) bond with a Wiberg bond order of 0.63. The DFT

TABLE VIII. Convergence of BSSE correction (in kcal/mol) from CCSD and (T) terms to the dissociation energies of $(LiH)_n$ clusters (n = 2–6).[a]

Species	Isomer	AwCVDZ	AwCVTZ	AwCVQZ	AVDZ	AVTZ	AVQZ
BSSE correction from all-electron ΔE_{CCSD}							
$(LiH)_2$		−0.779	−0.208	−0.059	−3.561	−2.499	−4.134
$(LiH)_3$	A	−1.505	−0.356	−0.103	−11.444	−4.704	−7.359
$(LiH)_4$	A	−2.126	−0.507	−0.148	−21.433	−7.070	−10.177
$(LiH)_4$	B	−3.251	−0.769	−0.226	−13.162	−9.642	−15.415
$(LiH)_5$	A	−2.775	−0.664	−0.193	−31.023	−9.403	−12.621
$(LiH)_5$	B	−4.024	−0.953	−0.276	−21.360	−12.555	−19.338
$(LiH)_6$	A	−4.693	−1.194	−0.345	−30.777	−17.274	−26.590
$(LiH)_6$	B	−4.385	−1.169	−0.353	−30.112	−16.573	−25.275
BSSE correction from all-electron $\Delta E_{(T)}$							
$(LiH)_2$		−0.010	−0.003	−0.001	−0.021	−0.019	−0.008
$(LiH)_3$		−0.017	−0.005	−0.001	−0.049	−0.031	−0.012
$(LiH)_4$	A	−0.023	−0.007	−0.001	−0.072	−0.043	−0.016
$(LiH)_4$	B	−0.040	−0.011	−0.002	−0.088	−0.066	−0.028
$(LiH)_5$	A	−0.028	−0.009	−0.002	−0.093	−0.055	−0.020
$(LiH)_5$	B	−0.048	−0.013	−0.003	−0.118	−0.081	−0.034
$(LiH)_6$	A	−0.096	−0.018	−0.002	−0.318	−0.196	−0.103
$(LiH)_6$	B	−0.069	−0.015	−0.002	−0.222	−0.142	−0.068

[a]CCSD/AVTZ optimized geometries are used throughout.

partial charges are +0.61 on Li and −0.61 on H. In the $(LiH)_2$ dimer, the structure consists of two Li atoms bridged by two H atoms. Each H atom interacts with two Li atoms through a 3-center, 2-electron (3c–2e) bond, and there is some overlap between the two σ orbitals. The resulting bond order is reduced to 0.21 per Li–H interaction. Furthermore, the partial charges on Li increase to +0.69, reflecting a higher concentration of electron density within the bridging orbitals.

The cyclic $(LiH)_n$ clusters (n = 3,4,5) are σ-delocalized, where multi-center bonding mitigates the electron deficiency of the system. In the cyclic $(LiH)_3$ trimer, three 3c–2e bonds are formed, with partial charges (±0.62) nearly identical to those of the LiH monomer. The computed bond orders (0.26) indicate that the electron density is delocalized across the Li–H–Li bridges rather than being confined to two-center bonds. This pattern persists in the cyclic $(LiH)_4$ and $(LiH)_5$ clusters, which feature four and five 3c–2e interactions, respectively. Across this series, the partial charges remain largely unchanged, decreasing slightly from ±0.62 in the trimer to ±0.59 in the pentamer. Therefore, as the ring expands, the electron density is effectively redistributed within the structure (Fig. 7).

Turning now to the compact structures, the $(LiH)_4$ cluster (isomer B) has four 4c–2e bonds with low bond orders (~0.15) and spatially extended σ orbitals. The partial charges are notably elevated (±0.66). A similar bonding profile is observed for Li_6H_6 (isomer A), which contains six 4c–2e bonds. A more noticeable change occurs in the asymmetric $(LiH)_5$ (isomer B) and $(LiH)_6$ (isomer B); in these species, the Li atoms become more internally coordinated, while the H atoms occupy the cluster surface. These structures exhibit a distribution of partial charges (Li: +0.59–0.66), with certain Li atoms being weaker bound to the hydride framework.

H. Aromaticity

σ-Aromaticity has been proposed as a contributing factor for stabilizing cyclic systems that lack a conventional π-electron framework, arising instead from the delocalization of σ electrons around a closed loop. Unlike π-aromaticity, σ-aromaticity is typically associated with small or highly constrained rings and has been invoked to rationalize the stability of systems such as cyclopropane and various inorganic analogues.[83] In our case, σ-aromaticity may contribute to the energetic preference for cyclic geometries in $(LiH)_n$ clusters, where electron delocalization occurs within the σ-bonding manifold.

Table IX lists our computed NICS values. At the ring centers (probe [a]), the isotropic NICS(0) values are small and only weakly negative (from −0.5 ppm to −0.2 ppm) for all cluster sizes considered, indicating that any ring-current effects are modest. This suggests that σ-aromatic stabilization is not driven by a strongly delocalized, collective ring current. In contrast, NICS(0) values at the midpoint of the Li–H bonds (probe [b]) are substantially more negative and decrease further with increasing cluster size, pointing to pronounced local σ-electron delocalization along the Li–H bonds.

This distinction is also supported by the $NICS(0)_{ijmax}$ values, which are negligible at the ring centers for $(LiH)_3$, $(LiH)_4$, and $(LiH)_5$ clusters but reach large negative values at the bond midpoints, consistent with strong anisotropic magnetic shielding associated with σ-bonding. The systematic increase in the magnitude of NICS(0) and $NICS(0)_{ijmax}$ from $(LiH)_2$ to $(LiH)_5$ indicates a cooperative enhancement of σ-electron delocalization as the clusters grow.

An apparent exception to the general trend is observed for the $(LiH)_2$ dimer, where the $NICS(0)_{ijmax}$ value at the ring center (probe [a]) takes the most negative value (−9.93 ppm). In the case of

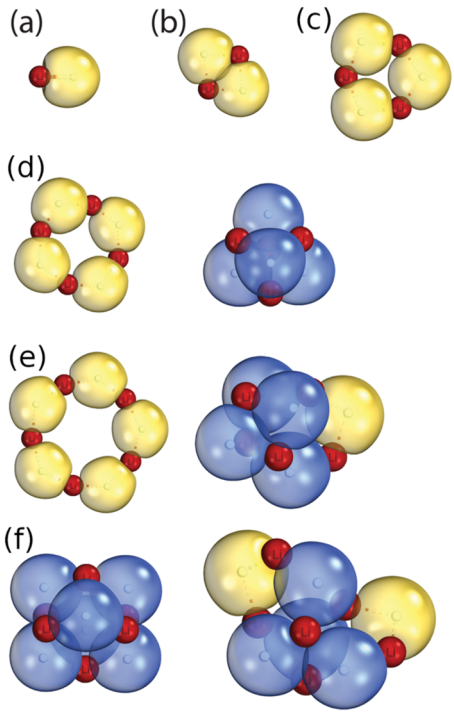

FIG. 7. Computed IBOs for the following lithium hydride species: (a) LiH, (b) $(LiH)_2$, (c) $(LiH)_3$, (d) $(LiH)_4$ isomers A and B, (e) $(LiH)_5$ (isomers A and B), and (f) $(LiH)_6$ (isomers A and B). The 3-center–2-electron (3c-2e) bonds are gold-colored, while the 4-center–2-electron (4c-2e) bonds are blue-colored.

TABLE IX. Computed NICS(0) (isotropic) and $NICS(0)_{ijmax}$ for cyclic $(LiH)_n$ clusters at the CCSD/AVTZ level. Values labeled [a] correspond to probe points located at the center of the rings and [b] were evaluated at the midpoint of the Li–H bonds. All values are given in ppm.

Cluster	$NICS(0)^{[a]}$	$NICS(0)^{[b]}$	$NICS(0)_{ijmax}^{[a]}$	$NICS(0)_{ijmax}^{[b]}$
$(LiH)_2$	−0.47	−4.36	−9.93	−10.46
$(LiH)_3$	−0.17	−5.46	−0.96	−12.77
$(LiH)_4$	−0.25	−5.79	−0.33	−13.74
$(LiH)_5$	−0.29	−5.88	−0.27	−14.35

$(LiH)_2$, the "ring center" is ambiguous as the system does not form a conventional cyclic framework but rather a small and highly constrained motif. Consequently, the probe position may lie near the Li–H bonds, capturing local σ-bonding shielding rather than a global ring current. As the size increases, the ring interior becomes more spatially defined and is "magnetically decoupled" from σ bonds, causing these values to diminish.

Overall, the magnetic aromaticity analysis is consistent with the bonding picture obtained from the IBO analysis in Sec. III G. The IBOs reveal extensive σ-electron delocalization through multi-center Li–H bonding rather than conventional two-center bonds. In line with this, the NICS results show only weakly negative values at the ring centers but significantly more negative values at the Li–H bond midpoints, indicating that the delocalization is predominantly local and bond-centered. The lack of a significant global NICS(0) signal at the geometric center suggests that these delocalized clusters do not exhibit classical aromaticity, like in benzene. Thus, stabilization in cyclic $(LiH)_n$ arises from σ-electron delocalization distributed over Li–H bridges rather than from a global ring current.

IV. SUMMARY AND CONCLUSIONS

This study presents high-level benchmark dissociation energies and total atomization energies of $(LiH)_n$ (n = 1–6) clusters. Our best estimates of energetics were obtained from composite *ab initio* methods, inspired by the W*n* and HEAT theories, which achieve CCSD(T)/CBS accuracy by rigorously accounting for core–valence correlation, basis set superposition error (BSSE), scalar relativistic effects, and the diagonal Born–Oppenheimer correction (DBOC). All investigated $(LiH)_n$ clusters are found to be bound relative to both their monomeric and atomic dissociation limits.

While Hartree–Fock captures most of the interaction, electron correlation effects, specifically the valence CCSD contribution, play a decisive role in stabilizing compact clusters over open cyclic rings. This dependence occurs even in smaller clusters. For example, the CCSD contribution to the dissociation energy of the cubane-like $(LiH)_4$ system (7.2 kcal/mol) is nearly seven times larger than that of its planar cyclic isomer (1.05 kcal/mol). Parenthetical triples (T) follow similar trends at a smaller magnitude, while core–valence correlation effects (ΔCV) further stabilize the clusters.

We find that, even though Li is a light atom, all-electron calculations on $(LiH)_n$ clusters require weighted core-valence basis sets (AwCV*n*Z) to avoid the pathological convergence of the basis set superposition error, which was observed with standard valence-only basis sets.

An assessment of various DFT methods indicates that they correctly predict the relative energetic ordering of the isomers. Notably, the revDSD-PBEP86-D4 double hybrid functional exhibits superior performance, attaining sub-kcal/mol accuracy for the energetics of $(LiH)_n$ clusters, relative to our CCSD(T)/CBS best estimates.

The many-body expansion (MBE) analysis of the interaction energy of the monocyclic clusters with respect to the LiH molecules reveals that the two- and three-body terms are consistently negative, while all higher-order terms are negligible, even though some of them are also negative.

Beyond energetics, structural analysis reveals that Li–H bonds contract systematically as the clusters grow in size and the Li–H–Li bond angles widen. This trend is driven by the relaxation of geometric constraints on multicenter bonding. In addition, the computed bond length for the diatomic LiH agrees with the experimental value.

Finally, intrinsic bond orbital (IBO) and nucleus-independent chemical shift (NICS) analyses reveal that stabilization in these electron-deficient systems is governed by multi-center σ-electron delocalization (3c–2e and 4c–2e bonds). This σ-aromaticity is local and bond-centered, rather than arising from a global ring current. Collectively, these results establish lithium hydride clusters as prototypical systems where electrostatics, electron correlation, and σ-delocalization jointly govern structure and stability.

SUPPLEMENTARY MATERIAL

DFT, MP2, CCSD, and CCSD(T) energies of $(LiH)_n$ clusters, MBE of dissociation energies, multireference diagnostics, excitation energies, and Cartesian coordinates (supplementary material).

ACKNOWLEDGMENTS

Calculations were carried out at the NKUA and NHRF HPC facilities; the most demanding CCSD(T) calculations were performed at the Chemfarm HPC cluster of the Weizmann Institute of Science. E.S. acknowledges computational resources and support from the Ben May Center for Chemical Theory and Computation at the Weizmann Institute of Science. E.S. also expresses gratitude to Professor Jan M. L. Martin and his research group for helpful discussions. E.A.R. acknowledges the Hellenic Foundation for Research and Innovation for the financial support of this project under the fifth Call for HFRI PhD Fellowships (Fellowship Number: 21044).

AUTHOR DECLARATIONS

Conflict of Interest

The authors have no conflicts to disclose.

Author Contributions

Emmanouil Semidalas: Data curation (lead); Formal analysis (equal); Investigation (equal); Methodology (equal); Resources (equal); Validation (equal); Visualization (equal); Writing – original draft (equal); Writing – review & editing (equal). **Filippos Drakopoulos**: Data curation (equal); Formal analysis (supporting); Investigation (equal). **E. Alexandros Routsi**: Data curation (equal); Formal analysis (equal); Investigation (equal); Visualization (supporting); Writing – original draft (equal). **Demeter Tzeli**: Conceptualization (lead); Formal analysis (equal); Investigation (equal); Methodology (equal); Project administration (equal); Resources (equal); Supervision (equal); Validation (equal); Visualization (equal); Writing – original draft (equal); Writing – review & editing (lead).

DATA AVAILABILITY

The data that support the findings of this study are available within the article.

REFERENCES

[1] W. C. Stwalley and W. T. Zemke, "Spectroscopy and structure of the lithium hydride diatomic molecules and ions," J. Phys. Chem. Ref. Data **22**(1), 87–112 (1993).
[2] M. S. Longair, "The post-recombination universe—The dark ages," in *Galaxy Formation* (Springer Berlin Heidelberg, Berlin, Heidelberg, 1998), pp. 363–378.
[3] B. Liu and V. Bromm, "Effect of lithium hydride on the cooling of primordial gas," Mon. Not. R. Astron. Soc. **476**(2), 1826–1834 (2018).
[4] D. Galli and F. Palla, "The chemistry of the early universe," Astron. Astrophys. **335**, 403–420 (1998).
[5] A. Goudelis, M. Pospelov, and J. Pradler, "Light particle solution to the cosmic lithium problem," Phys. Rev. Lett. **116**(21), 211303 (2016).
[6] D. N. Friedel, A. Kemball, and B. D. Fields, "The search for extragalactic lithium hydride," Astrophys. J. **738**(1), 37 (2011).
[7] B. D. Fields, "The primordial lithium problem," Annu. Rev. Nucl. Part. Sci. **61**(1), 47–68 (2011).
[8] M. Pospelov, "Particle physics catalysis of thermal big bang nucleosynthesis," Phys. Rev. Lett. **98**(23), 231301 (2007).
[9] D. J. Searles and E. I. von Nagy-Felsobuki, "*Ab initio* potential-energy surface of LiH_2^+ and its analytical representation," Phys. Rev. A (Coll. Park) **43**(7), 3365–3372 (1991).
[10] E. Bodo, F. A. Gianturco, R. Martinazzo, A. Forni, and M. Raimondi, "Spatial energetics of protonated LiH: Lower-lying potential energy surfaces from valence bond calculations," J. Phys. Chem. A **104**(51), 11972–11982 (2000).
[11] I. Pino, R. Martinazzo, and G. F. Tantardini, "Quasi-classical trajectory study of the adiabatic reactions occurring on the two lowest-lying electronic states of the LiH_2^+ system," Phys. Chem. Chem. Phys. **10**(36), 5545 (2008).
[12] E. Bodo, F. A. Gianturco, and R. Martinazzo, "Reactive behavior of the $[LiH_2]^+$ system II. Collision-induced dissociation and collinear reaction dynamics of LiH^++H from quantum time dependent calculations," J. Phys. Chem. A **105**(49), 10994–11000 (2001).
[13] R. Martinazzo, G. F. Tantardini, E. Bodo, and F. A. Gianturco, "Accurate potential energy surfaces for the study of lithium–hydrogen ionic reactions," J. Chem. Phys. **119**(21), 11241–11248 (2003).
[14] C. Sanz, E. Bodo, and F. A. Gianturco, "Energetics and structure of the bound states in a lithium complex: The $(LiH_2)^+$ electronic ground state," Chem. Phys. **314**(1–3), 135–142 (2005).
[15] W. P. Kraemer and V. Špirko, "Bound and low-lying quasi-bound rotation–vibration levels of the ground electronic state of LiH_2^+," Chem. Phys. **330**(1–2), 190–203 (2006).
[16] W. P. Kraemer and V. Špirko, "Vibrational energies of LiH_2^+ and LiD_2^+ in the $\tilde{A}^1\Sigma^+$ electronic state," J. Phys. Chem. A **115**(41), 11313–11320 (2011).
[17] X. He, S. Lv, T. Hayat, and K. Han, "Potential energy surfaces for the first two lowest-lying electronic states of the LiH_2^+ system, and dynamics of the H^+ + LiH $\rightleftharpoons$ H_2^+ + Li + reactions," J. Phys. Chem. A **120**(15), 2459–2470 (2016).
[18] C. F. Bender and E. R. Davidson, "Theoretical study of the LiH molecule," J. Chem. Phys. **49**(9), 4222–4229 (1968).
[19] M. Musiał and S. A. Kucharski, "First principle calculations of the potential energy curves for electronic states of the lithium dimer," J. Chem. Theory Comput. **10**(3), 1200–1211 (2014).
[20] S. Saidi, N. Mabrouk, J. Dhiflaoui, and H. Berriche, "Structural, spectroscopic, and dynamic properties of $Li_2^+(X_2\sum_g^+)$ in interaction with krypton atom," Molecules **28**(14), 5512 (2023).
[21] S. Nasiri and M. Zahedi, "A benchmark study of Li_2^+, Li_2^-, LiH^+ and LiH^-: Quantum Monte-Carlo and coupled-cluster computations," Comput. Theor. Chem. **1114**, 106–117 (2017).
[22] F. H. Welch, "Lithium hydride: A space age shielding material," Nucl. Eng. Des. **26**(3), 444–460 (1974).
[23] L. Wang, M. Z. Quadir, and K.-F. Aguey-Zinsou, "Direct and reversible hydrogen storage of lithium hydride (LiH) nanoconfined in high surface area graphite," Int. J. Hydrogen Energy **41**(40), 18088–18094 (2016).
[24] S. Banger, V. Nayak, and U. P. Verma, "Hydrogen storage in lithium hydride: A theoretical approach," J. Phys. Chem. Solids **115**, 6–17 (2018).
[25] E. Nemukula, C. B. Mtshali, and F. Nemangwele, "Metal hydrides for sustainable hydrogen storage: A review," Int. J. Energy Res. **2025**(1), 6300225.
[26] F. R. Manby, D. Alfe, and M. J. Gillan, "Extension of molecular electronic structure methods to the solid state: Computation of the cohesive energy of lithium hydride," Phys. Chem. Chem. Phys. **8**(44), 5178 (2006).
[27] K. Raghavachari, G. W. Trucks, J. A. Pople, and M. Head-Gordon, "A fifth-order perturbation comparison of electron correlation theories," Chem. Phys. Lett. **157**(6), 479–483 (1989).
[28] J. D. Watts, J. Gauss, and R. J. Bartlett, "Coupled-cluster methods with noniterative triple excitations for restricted open-shell Hartree–Fock and other general single determinant reference functions. Energies and analytical gradients," J. Chem. Phys. **98**(11), 8718–8733 (1993).
[29] R. Antoine, Ph. Dugourd, D. Rayane, E. Benichou, B. Vezin, and M. Broyer, "Evolution of the metallicity in the Li_nH_m clusters as a function of m: Evidence for a segregation," Z. Phys. D: At., Mol. Clusters **40**(1), 436–440 (1997).

[30]B. Vezin, Ph. Dugourd, D. Rayane, P. Labastie, C. Bordas, and M. Broyer, "Optical absorption of Li_nH clusters," Z. Phys. D: At., Mol. Clusters **26**(1), 290–292 (1993).
[31]M. Bertolus, V. Brenner, and P. Millié, "Are lithium hydride clusters purely ionic? Study using model potentials and density-functional theory," J. Chem. Phys. **115**(9), 4070–4079 (2001).
[32]X. Wang and L. Andrews, "Infrared spectra and theoretical calculations of lithium hydride clusters in solid hydrogen, neon, and argon," J. Phys. Chem. A **111**(27), 6008–6019 (2007).
[33]H. Kato, K. Hirao, and K. Akagi, "Theoretical study of the structure and stability of oligomers of lithium hydride," Inorg. Chem. **20**(11), 3659–3663 (1981).
[34]P. von Ragué Schleyer and J. A. Pople, "The reaction of lithium with hydrogen. A model *ab initio* study," Chem. Phys. Lett. **129**(5), 475–480 (1986).
[35]M. D. Esrafili, F. Elmi, and N. L. Hadipour, "Density functional theory study of binding energies, ^{7}Li nuclear magnetic shielding, and electric field gradient tensors on the small clusters of Li_nH_m ($m \le n \le 4$)," J. Theor. Comput. Chem. **06**(04), 959–973 (2007).
[36]J. Čížek, "On the correlation problem in atomic and molecular systems. Calculation of wavefunction components in Ursell-type expansion using quantum-field theoretical methods," J. Chem. Phys. **45**(11), 4256–4266 (1966).
[37]W. Skomorowski, F. Pawłowski, T. Korona, R. Moszynski, P. S. Żuchowski, and J. M. Hutson, "Interaction between LiH molecule and Li atom from state-of-the-art electronic structure calculations," J. Chem. Phys. **134**(11), 114109 (2011).
[38]F. Grein, "Dibridged, monobridged, Y-shaped and linear structures of A_2H_2 molecules, with A = H, Li, Be, B, C, N, O and F. From acetylene to vinylidene," Mol. Phys. **123**(2), e2356750 (2025).
[39]X.-Y. Hou, Y.-F. Yang, X.-H. Yin, X.-B. Liu, L.-J. Cui, and Z.-H. Cui, "Highly T_h-Symmetric $Li_{12}H_{13}^-$ cluster: An archimedean cage with cavity-bound hydrogen," Inorg. Chem. **65**(1), 351–359 (2026).
[40]B. Avramidis, H. P. Paudel, D. Alfonso, Y. Duan, and K. D. Jordan, "Ground state property calculations of LiH_n complexes using IBM Qiskit's quantum simulator," AIP Adv. **14**(3), 035047 (2024).
[41]A. Karton, E. Rabinovich, J. M. L. Martin, and B. Ruscic, "W4 theory for computational thermochemistry: In pursuit of confident sub-kJ/mol predictions," J. Chem. Phys. **125**(14), 144108 (2006).
[42]A. Karton, P. R. Taylor, and J. M. L. Martin, "Basis set convergence of post-CCSD contributions to molecular atomization energies," J. Chem. Phys. **127**(6), 064104 (2007).
[43]A. Tajti, P. G. Szalay, A. G. Császár, M. Kállay, J. Gauss, E. F. Valeev, B. A. Flowers, J. Vázquez, and J. F. Stanton, "HEAT: High accuracy extrapolated *ab initio* thermochemistry," J. Chem. Phys. **121**(23), 11599–11613 (2004).
[44]Y. J. Bomble, J. Vázquez, M. Kállay, C. Michauk, P. G. Szalay, A. G. Császár, J. Gauss, and J. F. Stanton, "High-accuracy extrapolated *ab initio* thermochemistry. II. Minor improvements to the protocol and a vital simplification," J. Chem. Phys. **125**(6), 064108 (2006).
[45]M. E. Harding, J. Vázquez, B. Ruscic, A. K. Wilson, J. Gauss, and J. F. Stanton, "High-accuracy extrapolated *ab initio* thermochemistry. III. Additional improvements and overview," J. Chem. Phys. **128**(11), 114111 (2008).
[46]J. F. Stanton, "Why CCSD(T) works: A different perspective," Chem. Phys. Lett. **281**(1–3), 130–134 (1997).
[47]L. Goerigk, A. Hansen, C. Bauer, S. Ehrlich, A. Najibi, and S. Grimme, "A look at the density functional theory zoo with the advanced GMTKN55 database for general main group thermochemistry, kinetics and noncovalent interactions," Phys. Chem. Chem. Phys. **19**(48), 32184–32215 (2017).
[48]T. Gould, "Diet GMTKN55' offers accelerated benchmarking through a representative subset approach," Phys. Chem. Chem. Phys. **20**(44), 27735–27739 (2018).
[49]J. Řezáč, K. E. Riley, and P. Hobza, "S66: A well-balanced database of benchmark interaction energies relevant to biomolecular structures," J. Chem. Theory Comput. **7**(8), 2427–2438 (2011).
[50]B. Brauer, M. K. Kesharwani, S. Kozuch, and J. M. L. Martin, "The S66x8 benchmark for noncovalent interactions revisited: Explicitly correlated *ab initio* methods and density functional theory," Phys. Chem. Chem. Phys. **18**(31), 20905–20925 (2016).
[51]G. Santra, E. Semidalas, N. Mehta, A. Karton, and J. M. L. Martin, "S66x8 noncovalent interactions revisited: New benchmark and performance of composite localized coupled-cluster methods," Phys. Chem. Chem. Phys. **24**(41), 25555–25570 (2022).
[52]E. Semidalas, G. Santra, N. Mehta, and J. M. L. Martin, "S66 noncovalent interactions benchmark re-examined: Composite localized coupled cluster approaches," AIP Conf. Proc. **2611**, 020016 (2022).
[53]M. S. Gordon, D. G. Fedorov, S. R. Pruitt, and L. V. Slipchenko, "Fragmentation methods: A route to accurate calculations on large systems," Chem. Rev. **112**(1), 632–672 (2012).
[54]D. Tzeli and S. S. Xantheas, "The many-body expansion: From hydrogen bonded to light nuclear systems," Adv. Quantum Chem. **92**, 95–120 (2025).
[55]M. A. Collins and R. P. A. Bettens, "Energy-based molecular fragmentation methods," Chem. Rev. **115**(12), 5607–5642 (2015).
[56]R. M. Richard, K. U. Lao, and J. M. Herbert, "Understanding the many-body expansion for large systems. I. Precision considerations," J. Chem. Phys. **141**(1), 014108 (2014).
[57]K. U. Lao, K.-Y. Liu, R. M. Richard, and J. M. Herbert, "Understanding the many-body expansion for large systems. II. Accuracy considerations," J. Chem. Phys. **144**(16), 164105 (2016).
[58]D. Tzeli and S. S. Xantheas, "Breaking covalent bonds in the context of the many-body expansion (MBE). I. The purported 'first row anomaly' in XH_n (X = C, Si, Ge, Sn; n = 1–4)," J. Chem. Phys. **156**(24), 244303 (2022).
[59]J. Mato, D. Tzeli, and S. S. Xantheas, "The many-body expansion for metals. I. The alkaline earth metals Be, Mg, and Ca," J. Chem. Phys. **157**(8), 084313 (2022).
[60]D. Tzeli, J. Mato, and S. S. Xantheas, "The many-body expansion for metals: II. Nonadditive terms in clusters composed of metals with ns^1, ns^2, and ns^2p^1 configurations," J. Phys. Chem. A **129**(16), 3648–3662 (2025).
[61]T. Depastas, G. A. Souliotis, D. Tzeli, and S. S. Xantheas, "Many-body expansion for light nuclear systems," Phys. Rev. C **107**(4), 044004 (2023).
[62]S. Grimme, J. Antony, S. Ehrlich, and H. Krieg, "A consistent and accurate *ab initio* parametrization of density functional dispersion correction (DFT-D) for the 94 elements H-Pu," J. Chem. Phys. **132**(15), 154104 (2010).
[63]S. Grimme, S. Ehrlich, and L. Goerigk, "Effect of the damping function in dispersion corrected density functional theory," J. Comput. Chem. **32**(7), 1456–1465 (2011).
[64]F. Weigend and R. Ahlrichs, "Balanced basis sets of split valence, triple zeta valence and quadruple zeta valence quality for H to Rn: Design and assessment of accuracy," Phys. Chem. Chem. Phys. **7**(18), 3297–3305 (2005).
[65]D. Rappoport and F. Furche, "Property-optimized Gaussian basis sets for molecular response calculations," J. Chem. Phys. **133**(13), 134105 (2010).
[66]A. D. Becke, "Density-functional thermochemistry. III. The role of exact exchange," J. Chem. Phys. **98**(7), 5648–5652 (1993).
[67]P. J. Stephens, F. J. Devlin, C. F. Chabalowski, and M. J. Frisch, "*Ab initio* calculation of vibrational absorption and circular dichroism spectra using density functional force fields," J. Phys. Chem. **98**(45), 11623–11627 (1994).
[68]F. Neese, "Software update: The ORCA program system—version 6.0," WIREs Comput. Mol. Sci. **15**(2), e70019 (2025).
[69]F. Weigend, "Accurate Coulomb-fitting basis sets for H to Rn," Phys. Chem. Chem. Phys. **8**(9), 1057 (2006).
[70]A. Hellweg, C. Hättig, S. Höfener, and W. Klopper, "Optimized accurate auxiliary basis sets for RI-MP2 and RI-CC2 calculations for the atoms Rb to Rn," Theor. Chem. Acc. **117**(4), 587–597 (2007).
[71]F. Neese, F. Wennmohs, A. Hansen, and U. Becker, "Efficient, approximate and parallel Hartree–Fock and hybrid DFT calculations. A 'chain-of-spheres' algorithm for the Hartree–Fock exchange," Chem. Phys. **356**(1–3), 98–109 (2009).
[72]B. Helmich-Paris, B. de Souza, F. Neese, and R. Izsák, "An improved chain of spheres for exchange algorithm," J. Chem. Phys. **155**(10), 104109 (2021).
[73]R. Izsák and F. Neese, "An overlap fitted chain of spheres exchange method," J. Chem. Phys. **135**(14), 144105 (2011).
[74]F. Neese, "The SHARK integral generation and digestion system," J. Comput. Chem. **44**(3), 381–396 (2023).
[75]T. H. Dunning, "Gaussian basis sets for use in correlated molecular calculations. I. The atoms boron through neon and hydrogen," J. Chem. Phys. **90**(2), 1007–1023 (1989).

[76]R. A. Kendall, T. H. Dunning, and R. J. Harrison, "Electron affinities of the first-row atoms revisited. Systematic basis sets and wave functions," J. Chem. Phys. **96**(9), 6796–6806 (1992).
[77]D. E. Woon and T. H. Dunning, "Gaussian basis sets for use in correlated molecular calculations. III. The atoms aluminum through argon," J. Chem. Phys. **98**(2), 1358–1371 (1993).
[78]T. H. Dunning, K. A. Peterson, and A. K. Wilson, "Gaussian basis sets for use in correlated molecular calculations. X. The atoms aluminum through argon revisited," J. Chem. Phys. **114**(21), 9244–9253 (2001).
[79]H.-J. Werner, P. J. Knowles, F. R. Manby, J. A. Black, K. Doll, A. Heßelmann, D. Kats, A. Köhn, T. Korona, D. A. Kreplin, Q. Ma, T. F. Miller, A. Mitrushchenkov, K. A. Peterson, I. Polyak, G. Rauhut, and M. Sibaev, "The Molpro quantum chemistry package," J. Chem. Phys. **152**(14), 144107 (2020).
[80]P. J. Knowles, C. Hampel, and H.-J. Werner, "Coupled cluster theory for high spin, open shell reference wave functions," J. Chem. Phys. **99**(7), 5219–5227 (1993).
[81]D. Feller, K. A. Peterson, and T. D. Crawford, "Sources of error in electronic structure calculations on small chemical systems," J. Chem. Phys. **124**(5), 054107 (2006).
[82]F. Weinhold and C. Landis, *Discovering Chemistry with Natural Bond Orbitals* (Wiley, 2012).
[83]Z. Chen, C. S. Wannere, C. Corminboeuf, R. Puchta, P. v. R. Schleyer, and R. Schleyer, "Nucleus-independent chemical shifts (NICS) as an aromaticity criterion," Chem. Rev. **105**(10), 3842–3888 (2005).
[84]R. Ditchfield, "Self-consistent perturbation theory of diamagnetism," Mol. Phys. **27**(4), 789–807 (1974).
[85]K. Aidas, C. Angeli, K. L. Bak, V. Bakken, R. Bast, L. Boman, O. Christiansen, R. Cimiraglia, S. Coriani, P. Dahle, E. K. Dalskov, U. Ekström, T. Enevoldsen, J. J. Eriksen, P. Ettenhuber, B. Fernández, L. Ferrighi, H. Fliegl, L. Frediani, K. Hald, A. Halkier, C. Hättig, H. Heiberg, T. Helgaker, A. C. Hennum, H. Hettema, E. Hjertenæs, S. Høst, I. M. Høyvik, M. F. Iozzi, B. Jansík, H. J. A. Jensen, D. Jonsson, P. Jørgensen, J. Kauczor, S. Kirpekar, T. Kjærgaard, W. Klopper, S. Knecht, R. Kobayashi, H. Koch, J. Kongsted, A. Krapp, K. Kristensen, A. Ligabue, O. B. Lutnæs, J. I. Melo, K. V. Mikkelsen, R. H. Myhre, C. Neiss, C. B. Nielsen, P. Norman, J. Olsen, J. M. H. Olsen, A. Osted, M. J. Packer, F. Pawlowski, T. B. Pedersen, P. F. Provasi, S. Reine, Z. Rinkevicius, T. A. Ruden, K. Ruud, V. V. Rybkin, P. Sałek, C. C. M. Samson, A. S. de Merás, T. Saue, S. P. A. Sauer, B. Schimmelpfennig, K. Sneskov, A. H. Steindal, K. O. Sylvester-Hvid, P. R. Taylor, A. M. Teale, E. I. Tellgren, D. P. Tew, A. J. Thorvaldsen, L. Thøgersen, O. Vahtras, M. A. Watson, D. J. D. Wilson, M. Ziolkowski, and H. Ågren, "The Dalton quantum chemistry program system," WIREs Comput. Mol. Sci. **4**(3), 269–284 (2014).
[86]J. M. L. Martin and G. de Oliveira, "Towards standard methods for benchmark quality *ab initio* thermochemistry—W1 and W2 theory," J. Chem. Phys. **111**(5), 1843–1856 (1999).
[87]K. A. Peterson and T. H. Dunning, "Accurate correlation consistent basis sets for molecular core–valence correlation effects: The second row atoms Al–Ar, and the first row atoms B–Ne revisited," J. Chem. Phys. **117**(23), 10548–10560 (2002).
[88]M. Born and R. Oppenheimer, "Zur Quantentheorie der Molekeln," Ann. Phys. **389**(20), 457–484 (1927).
[89]A. Karton and J. M. L. Martin, "Comment on: 'Estimating the Hartree-Fock limit from finite basis set calculations' [Jensen F (2005) Theor Chem Acc 113:267]," Theor. Chem. Acc. **115**(4), 330–333 (2006).
[90]D. W. Schwenke, "The extrapolation of one-electron basis sets in electronic structure calculations: How it should work and how it can be made to work," J. Chem. Phys. **122**(1), 014107 (2005).
[91]A. Halkier, T. Helgaker, P. Jørgensen, W. Klopper, H. Koch, J. Olsen, and A. K. Wilson, "Basis-set convergence in correlated calculations on Ne, N_2, and H_2O," Chem. Phys. Lett. **286**(3–4), 243–252 (1998).
[92]T. Helgaker, W. Klopper, H. Koch, and J. Noga, "Basis-set convergence of correlated calculations on water," J. Chem. Phys. **106**(23), 9639–9646 (1997).
[93]D. Peng and M. Reiher, "Exact decoupling of the relativistic Fock operator," Theor. Chem. Acc. **131**(1), 1081 (2012).
[94]W. A. De Jong, R. J. Harrison, and D. A. Dixon, "Parallel Douglas–Kroll energy and gradients in NWChem: Estimating scalar relativistic effects using Douglas–Kroll contracted basis sets," J. Chem. Phys. **114**(1), 48–53 (2001).
[95]J. M. L. Martin and N. Sylvetsky, "A simple model for scalar relativistic corrections to molecular total atomisation energies," Mol. Phys. **117**(17), 2225–2232 (2019).
[96]D. A. Matthews, L. Cheng, M. E. Harding, F. Lipparini, S. Stopkowicz, T.-C. Jagau, P. G. Szalay, J. Gauss, and J. F. Stanton, "Coupled-cluster techniques for computational chemistry: The CFOUR program package," J. Chem. Phys. **152**(21), 214108 (2020).
[97]J. H. Thorpe, C. A. Lopez, T. L. Nguyen, J. H. Baraban, D. H. Bross, B. Ruscic, and J. F. Stanton, "High-accuracy extrapolated *ab initio* thermochemistry. IV. A modified recipe for computational efficiency," J. Chem. Phys. **150**(22), 224102 (2019).
[98]A. D. Boese, M. Oren, O. Atasoylu, J. M. L. Martin, M. Kállay, and J. Gauss, "W3 theory: Robust computational thermochemistry in the kJ/mol accuracy range," J. Chem. Phys. **120**, 4129–4141 (2004).
[99]K. A. Peterson, D. Feller, and D. A. Dixon, "Chemical accuracy in *ab initio* thermochemistry and spectroscopy: Current strategies and future challenges," Theor. Chem. Acc. **131**(1), 1079 (2012).
[100]A. Karton, "A computational chemist's guide to accurate thermochemistry for organic molecules," WIREs Comput. Mol. Sci. **6**(3), 292–310 (2016).
[101]S. J. Klippenstein, L. B. Harding, and B. Ruscic, "*Ab initio* computations and active thermochemical tables hand in hand: Heats of formation of core combustion species," J. Phys. Chem. A **121**(35), 6580–6602 (2017).
[102]H. Sellers and P. Pulay, "The adiabatic correction to molecular potential surfaces in the SCF approximation," Chem. Phys. Lett. **103**(6), 463–465 (1984).
[103]J. H. Thorpe and J. F. Stanton, "Hartree–Fock instabilities and the diagonal Born–Oppenheimer correction," Mol. Phys. **118**(19–20), e1742936 (2020).
[104]S. F. Boys and F. Bernardi, "The calculation of small molecular interactions by the differences of separate total energies. Some procedures with reduced errors," Mol. Phys. **19**(4), 553–566 (1970).
[105]L. Turi and J. J. Dannenberg, "Correcting for basis set superposition error in aggregates containing more than two molecules: Ambiguities in the calculation of the counterpoise correction," J. Phys. Chem. **97**(11), 2488–2490 (1993).
[106]W. Klopper, M. Schütz, H. P. Lüthi, and S. Leutwyler, "An *ab initio* derived torsional potential energy surface for $(H_2O)_3$. II. Benchmark studies and interaction energies," J. Chem. Phys. **103**(3), 1085–1098 (1995).
[107]V. Fishman, E. Semidalas, and J. M. L. Martin, "Basis set extrapolation from the vanishing counterpoise correction condition," J. Phys. Chem. A **128**(35), 7462–7470 (2024).
[108]T. J. Lee and P. R. Taylor, "A diagnostic for determining the quality of single-reference electron correlation methods," Int. J. Quantum Chem. **36**(S23), 199–207 (1989).
[109]C. L. Janssen and I. M. B. Nielsen, "New diagnostics for coupled-cluster and Møller–Plesset perturbation theory," Chem. Phys. Lett. **290**(4–6), 423–430 (1998).
[110]M. L. Leininger, I. M. B. Nielsen, T. D. Crawford, and C. L. Janssen, "A new diagnostic for open-shell coupled-cluster theory," Chem. Phys. Lett. **328**(4–6), 431–436 (2000).
[111]T. J. Lee, "Comparison of the T_1 and D_1 diagnostics for electronic structure theory: A new definition for the open-shell D_1 diagnostic," Chem. Phys. Lett. **372**(3–4), 362–367 (2003).
[112]A. Najibi and L. Goerigk, "DFT-D4 counterparts of leading meta-generalized-gradient approximation and hybrid density functionals for energetics and geometries," J. Comput. Chem. **41**(30), 2562–2572 (2020).
[113]Y. Zhao and D. G. Truhlar, "The M06 suite of density functionals for main group thermochemistry, thermochemical kinetics, noncovalent interactions, excited states, and transition elements: Two new functionals and systematic testing of four M06-class functionals and 12 other functionals," Theor. Chem. Acc. **120**(1–3), 215–241 (2008).
[114]G. Santra, N. Sylvetsky, and J. M. L. Martin, "Minimally empirical double-hybrid functionals trained against the GMTKN55 database: revDSD-PBEP86-D4, revDOD-PBE-D4, and DOD-SCAN-D4," J. Phys. Chem. A **123**(24), 5129–5143 (2019).
[115]E. Caldeweyher, S. Ehlert, A. Hansen, H. Neugebauer, S. Spicher, C. Bannwarth, and S. Grimme, "A generally applicable atomic-charge dependent London dispersion correction," J. Chem. Phys. **150**(15), 154122 (2019).

[116]E. Caldeweyher, J.-M. Mewes, S. Ehlert, and S. Grimme, "Extension and evaluation of the D4 London-dispersion model for periodic systems," Phys. Chem. Chem. Phys. **22**(16), 8499–8512 (2020).
[117]E. J. Baerends, D. E. Ellis, and P. Ros, "Self-consistent molecular Hartree–Fock–Slater calculations I. The computational procedure," Chem. Phys. **2**(1), 41–51 (1973).
[118]O. Vahtras, J. Almlöf, and M. W. Feyereisen, "Integral approximations for LCAO-SCF calculations," Chem. Phys. Lett. **213**(5–6), 514–518 (1993).
[119]K. P. Huber and G. Herzberg, "IV. Constants of diatomic molecules," in *Molecular Spectra and Molecular Structure*, edited by K. P. Huber and G. Herzberg (Springer US, Boston, MA, 1979), pp. 8–689.
[120]E. Semidalas, A. Karton, and J. M. L. Martin, "W4Λ: Leveraging Λ coupled-cluster for accurate computational thermochemistry approaches," J. Phys. Chem. A **128**(9), 1715–1724 (2024).
[121]J. M. L. Martin and S. Parthiban, "W1 and W2 theories, and their variants: Thermochemistry in the kJ/mol accuracy range," in *Quantum-Mechanical Prediction of Thermochemical Data*, edited by J. Cioslowski (Kluwer Academic Publishers, Dordrecht, 2002), pp. 31–65.
[122]A. Karton and J. M. L. Martin, "Explicitly correlated Wn theory: W1-F12 and W2-F12," J. Chem. Phys. **136**(12), 124114 (2012).
[123]J. H. Thorpe, J. L. Kilburn, D. Feller, P. B. Changala, D. H. Bross, B. Ruscic, and J. F. Stanton, "Elaborated thermochemical treatment of HF, CO, N_2, and H_2O: Insight into HEAT and its extensions," J. Chem. Phys. **155**(18), 184109 (2021).
[124]J. H. Thorpe, P. R. Franke, J. F. Stanton, D. H. Bross, and B. Ruscic, "Reducing the cost of CCSD basis set extrapolation in *ab initio* computational thermochemistry," J. Chem. Theory Comput. **22**(4), 1931–1946 (2026).
[125]A. Karton, N. Sylvetsky, and J. M. L. Martin, "W4-17: A diverse and high-confidence dataset of atomization energies for benchmarking high-level electronic structure methods," J. Comput. Chem. **38**(24), 2063–2075 (2017).
[126]A. Karton, S. Daon, and J. M. L. Martin, "W4-11: A high-confidence benchmark dataset for computational thermochemistry derived from first-principles W4 data," Chem. Phys. Lett. **510**(4–6), 165–178 (2011).
[127]F. H. Crawford and T. Jorgensen, "The band spectra of the hydrides of lithium. Part III. Potential curves and isotope relations," Phys. Rev. **49**(10), 745–752 (1936).
[128]P. Kraus, "Basis set extrapolations for density functional theory," J. Chem. Theory Comput. **16**(9), 5712–5722 (2020).
[129]P. Kraus, "Extrapolating DFT toward the complete basis set limit: Lessons from the PBE family of functionals," J. Chem. Theory Comput. **17**(9), 5651–5660 (2021).
[130]N. Mehta and J. M. L. Martin, "Explicitly correlated double-hybrid DFT: A comprehensive analysis of the basis set convergence on the GMTKN55 database," J. Chem. Theory Comput. **18**(10), 5978–5991 (2022).
[131]J. P. Heindel, K. M. Herman, E. Aprà, and S. S. Xantheas, "Guest–Host interactions in clathrate hydrates: Benchmark MP2 and CCSD(T)/CBS binding energies of CH_4, CO_2, and H_2S in $(H_2O)_{20}$ cages," J. Phys. Chem. Lett. **12**, 7582 (2021).
[132]J. P. Heindel and S. S. Xantheas, "The many-body expansion for aqueous systems revisited: II. Alkali metal and halide ion–water interactions," J. Chem. Theory Comput. **17**(4), 2200–2216 (2021).
[133]J. P. Heindel, Q. Yu, J. M. Bowman, and S. S. Xantheas, "Benchmark electronic structure calculations for $H_3O^+(H_2O)_n$, n = 0–5, clusters and tests of an existing 1,2,3-body potential energy surface with a new 4-body correction," J. Chem. Theory Comput. **14**(9), 4553–4566 (2018).
[134]C. K. Egan and F. Paesani, "Assessing many-body effects of water self-ions. I: $OH^-(H_2O)_n$ clusters," J. Chem. Theory Comput. **14**(4), 1982–1997 (2018).
[135]C. K. Egan and F. Paesani, "Assessing many-body effects of water self-ions. II: H_3O^+ $(H_2O)_n$ clusters," J. Chem. Theory Comput. **15**(9), 4816–4833 (2019).
[136]M. Hargittai and Z. Varga, "Molecular constants of aluminum monohalides: Caveats for computations of simple inorganic molecules," J. Phys. Chem. A **111**(1), 6–8 (2007).
[137]D. Tzeli and A. A. Tsekouras, "Mind the basis set superposition error," Chem. Phys. Lett. **496**(1–3), 42–45 (2010).
[138]G. Knizia, "Intrinsic atomic orbitals: An unbiased bridge between quantum theory and chemical concepts," J. Chem. Theory Comput. **9**(11), 4834–4843 (2013).
[139]J. P. Perdew, K. Burke, and M. Ernzerhof, "Generalized gradient approximation made simple," Phys. Rev. Lett. **77**(18), 3865–3868 (1996).
[140]J. P. Perdew, K. Burke, and M. Ernzerhof, "Generalized gradient approximation made simple [Phys. Rev. Lett. 77, 3865 (1996)]; Erratum," Phys. Rev. Lett. **78**(7), 1396 (1997).
[141]K. B. Wiberg, "Application of the pople-santry-segal CNDO method to the cyclopropylcarbinyl and cyclobutyl cation and to bicyclobutane," Tetrahedron **24**(3), 1083–1096 (1968).